SLAC-PUB-2244
October 1978
(E/I)

A SOURCE OF HIGHLY POLARIZED ELECTRONS AT THE STANFORD LINEAR ACCELERATOR CENTER*

M. J. Alguard[†], J. E. Clendenin, R. D. Ehrlich[‡], V. W. Hughes, J. S. Ladish[#] and M. S. Lubell
Gibbs Laboratory, Physics Department
Yale University, New Haven, Connecticut 06520

K. P. Schüler
Gibbs Laboratory, Physics Department
Yale University, New Haven, Connecticut 06520
and
Fakultät für Physik, Universität Bielefeld
D-4800 Bielefeld, West Germany

G. Baum and W. Raith
Fakultät für Physik, Universität Bielefeld
D-4800 Bielefeld, West Germany

R. H. Miller
Stanford Linear Accelerator Center
Stanford University, Stanford, California 94305

with an Appendix by

W. Lysenko[#]
Gibbs Laboratory, Physics Department
Yale University, New Haven, Connecticut 06520

(Submitted to Nucl. Instrum. Methods.)

*Research (Yale report no. COO-3075-186) supported in part by the Department of Energy under contract nos. EY-76-C-02-3075 (Yale) and EY-76-C-03-0515 (SLAC), the U.S. Office of Naval Research under contract no. N00014-76-C-0007, the German Federal Ministry of Research and Technology, and the University of Bielefeld.

[†]Present address: Department of Electrical Engineering, Stanford University, Stanford, CA 94305.

[‡]Present address: Department of Physics, Cornell University, Ithaca, NY 14850

[#]Present address: Los Alamos Scientific Laboratory, Los Alamos, NM 87545

ABSTRACT

A polarized electron source based upon photoionization of a state-selected ^{6}Li atomic beam has been developed as an injection gun for the Stanford two-mile electron linear accelerator. The source (PEGGY) produces a pulsed beam of electrons with a maximum intensity of 2.6×10^{9} electrons per pulse, a polarization of 0.85, a pulse length of 1.6 μsec, and a repetition rate of 180 pulses/sec. Since its installation at SLAC in July 1974, PEGGY has been used in several high energy electron-nucleon scattering experiments.

SECTION 1

INTRODUCTION

High energy polarized electron beams have been used in a number of experiments in the last five years. Together with polarized nucleon targets, experiments with polarized electron beams 1-3) provide a means for examining models of the spin structure of nucleons 4-11) and for testing sum rules 12) and scaling principles 13,14), as well as for investigating the spin dependence of specific electroproduction channels 15,16). Furthermore, high energy polarized electron scattering experiments with unpolarized nucleon targets 2,17-19) provide a means for studying parity nonconserving (PNC) effects of the neutral weak current. (See for example Refs. 20-22.)

With the study of the spin structure of the proton as its primary goal, the development of the first source of polarized electrons used in a high energy physics experiment was begun in 1971. This source, PEGGY, which is based on the photoionization of polarized lithium atoms, was developed at Yale University during the period 1971-1974 for use at the Stanford Linear Accelerator Center (SLAC). PEGGY was moved to SLAC early in 1974 and the polarized beam was first injected into the linac during the summer. In November 1974,

Møller scattering studies at GeV energies were performed to measure the polarization after acceleration 23). High energy scattering experiments with a polarized-proton target were begun several months later. Data on elastic 1), deep inelastic 2,3), and resonance region 24) scattering of longitudinally polarized protons have by now been obtained. A search was also made with PEGGY for PNC effects in the scattering of longitudinally polarized electrons by unpolarized nuclei 2,18).

In this paper we report on the physical and technological details of PEGGY. In the remaining parts of Section 1 we will review the requirements imposed on a polarized electron source by the SLAC accelerator and by the high energy experiments. We will also provide a brief survey of developed methods for producing polarized electrons. In Section 2 we will describe the method employed in producing and in measuring the electron polarization of the PEGGY beam. In Section 3 we will describe in some detail the PEGGY apparatus, and we will conclude in Section 4 with a discussion of the performance of the source and some observations about future developments.

1.1 REQUIREMENTS OF SOURCES

The performance characteristics which can be used to classify polarized electron sources have been discussed by a

number of authors 25-32). The electron polarization, $\vec{P}_e$, is defined as the ensemble average of the expectation value of the Pauli spin operator in the rest frame of the electron. For a longitudinally polarized electron beam the magnitude of the polarization, P_e, is given by $P_e = (n^+ - n^-)/(n^+ + n^-)$ in which n^+ (n^-) is the number of electrons in the beam with spin parallel (antiparallel) to the beam direction. Scattering experiments with polarized electron beams generally involve the measurement of cross sections or counting rate asymmetries for opposite orientations of $\vec{P}_e$. The measured asymmetry, Δ, defined by

$$\Delta = \frac{N_+ - N_-}{N_+ + N_-} \tag{1}$$

for counting rates N_+ and N_-, corresponding to the two orientations of $\vec{P}_e$, is related to the asymmetry for a fully polarized beam, A, by

$$A = \Delta / P_e \quad . \tag{2}$$

For a polarized electron beam of intensity I_e the statistical error, δA, in a measurement of A is

$$\delta A \propto 1/\zeta \tag{3}$$

where ζ is a figure of merit given by

$$\zeta = P_e I_e^{1/2} \quad . \tag{4}$$

Another important characteristic is the emittance of the electron beam. If a magnetic field, H, is present in an electron source, but absent elsewhere, the emittance must account for the influence of the magnetic vector potential on the canonical angular momentum 33). The result is the generalized emittance, ε^*, given by

$$\varepsilon^* \simeq \rho\,(v/v')\left[1 + \frac{1}{2}\,(e/m)\rho\,H/v\right] \qquad \text{(MKSA units)} \qquad (5)$$

where v is the average initial electron velocity of the photoelectrons in the source volume, ρ is the radius of the source volume, v′ is the average velocity of the beam after extraction, and e and m are the charge and mass of the electron. Additional performance characteristics generally considered include energy spread, ΔE, stability and reliability, and, for a pulsed source, the pulse length and repetition rate. Furthermore, the performance of a polarized electron source must be judged by the ease and speed of beam polarization reversal and by the variation of beam intensity and polarization associated with such reversals.

For high energy polarized electron experiments, the characteristics required of a polarized electron source are determined by the experiment itself and by the accelerator into which the polarized beam is injected. The Stanford two-mile linear accelerator 34) is a pulsed rf electron accelerator capable of achieving peak beam currents of 60 mA

in a 1.6 μs pulse at a repetition rate of ≤360 pps for beam energies up to ~22 GeV. During recent years, however, the accelerator usually has been operated at a repetition rate of 180 pps with beam sharing on a pulse to pulse basis generally limiting a single experiment to ≤120 pps. The injector of the accelerator is designed to accept ~70 keV electrons with a FWHM energy spread of ≤1.5 keV and an emittance of ~7 mrad-cm 35). Efficient beam transport through the accelerator requires an intensity of at least $\sim 3 \times 10^8$ electrons/pulse because of the limited sensitivity of the linac beam monitors. Finally, the source must be designed to meet the vacuum requirements of the accelerator: freedom from hydrocarbon contamination and use of bakeable ultra-high vacuum materials.

While many experiments can utilize high beam intensities, experiments with polarized nucleon targets are restricted to relatively low average intensities because of the radiation damage to the target by the incident electron beam. For such experiments an electron beam polarization close to unity is very important in order to achieve a high figure of merit. (For the experiments at SLAC with the Yale/SLAC butanol polarized-proton target 1,36), the 1/e depolarizing dose was $\sim 10^{15}$ electrons. With a beam intensity of $\sim 10^9$ electrons/pulse at 120 pps incident on the target, the data were accumulated in ~2 h periods separated by ~3/4 h intervals for target annealing/changing and repolarizing.)

Experimental applications also place requirements on the reversal of the direction of polarization. If small asymmetries are to be measured, the polarization must be reversed at frequent intervals to avoid systematic effects associated with long-term drifts. Under polarization reversal the beam energy, intensity and position at the target should remain constant.

1.2 SURVEY OF POLARIZED ELECTRON SOURCES

The development of sources of polarized electrons dates back to the proposals of Fues and Hellman in 1930 37), but has been actively pursued only since the late 1950's. Polarized electron source development has been the subject of numerous monographs and review papers. (See Refs. 28,30) and references therein.)

By 1971, when a polarized electron source was proposed for SLAC 38), there were only four techniques which had undergone sufficient development for them to be considered potential candidates for accelerator applications. Low-energy Mott scattering from atoms had been investigated at Mainz 39,40), at Karlsruhe 41-44), and at Stanford 45). The technique of extracting electrons from an optically pumped helium discharge had been developed at Rice 46). The photoionization of high-Z alkali atoms by circularly polarized light (the Fano effect) had been investigated at Yale 47,48)

and at Karlsruhe 49,50). The photoionization of state-selected alkali atoms was studied at Yale 26,51) and at Bonn 52). Only the latter two methods seemed to be viable choices for the SLAC source. Since the work on photoionization of state-selected alkali atoms at Yale had already reached the stage of a prototype operating in a pulsed mode at 100 keV, it was decided to construct PEGGY based upon this method.

Since 1971, further development of polarized electron sources has occurred. Fano effect sources have been developed at Bonn 53,54) for use with the 2 GeV electron-synchrotron 55) and at Yale 32) for low-energy electron scattering experiments 56). Sources based on photoemission from GaAs 29,57) and field emission from a tungsten tip covered with ferromagnetic EuS 31,58) have been developed. In addition, electron polarization in low energy diffraction (LEED) from tungsten and gold crystals has been studied 59-62). A GaAs photoemission source which has produced up to 4×10^{11} electrons/pulse on target with a polarization of ~ 0.4 is now also being used at SLAC with an unpolarized target for a PNC experiment 19). The present status of polarized electron sources is summarized in Table I.

SECTION 2

METHOD

2.1 PHOTOIONIZATION OF STATE-SELECTED ^{6}LI

The production of polarized electrons by the photoionization of state-selected ^{6}Li atoms in an atomic beam is discussed in Refs. 26, 63). In this section the salient points of the method, which is illustrated in Fig. 1, will be reviewed.

A beam of ^{6}Li atoms is produced by heating and vaporizing lithium metal in an oven and passing the emerging atoms through a collimation system. Atoms in the $m_J = +1/2$ ground state are selected by deflection in the strong inhomogeneous field of a sextupole magnet,* resulting in an atomic beam with an electronic polarization, $\vec{P}_{e,atom}$, of magnitude close to unity. The state-selected atoms adiabatically enter an ionization region in which there is an ~200-G longitudinal magnetic field with $\vec{P}_{e,atom}$ following the field direction and remaining close to unity. If the direction of the longitudinal magnetic field is reversed, the direction of

---

*Depolarization of atoms crossing the zero-field axis of the sextupole magnet (Majorana transitions) can be neglected in the present case 64).

$\vec{P}_{e,atom}$ is reversed with respect to the direction of the beam.

The magnitude of the electronic polarization of the atoms, $P_{e,atom}$, can be written as a function of the magnetic field, H, in the ionization region according to

$$P_{e,atom} = s\, f(H) \quad , \tag{6}$$

where s is the sextupole state selection parameter given by

$$s = \frac{\Omega^+ - \Omega^-}{\Omega^+ + \Omega^-} \tag{7}$$

with $\Omega^\pm$ the effective solid angle for transmission of the $m_J = \pm 1/2$ atoms through the sextupole magnet. As can be seen from Fig. 2, s varies with the assumed radial extent, ρ, of the ionization region. For PEGGY, the ionization region is estimated to have a radius of $\rho = 0.30 \pm 0.15$ cm. (See Section 3.4.) The corresponding value of s is $s = 0.97 \pm 0.03$ which includes an error of ~0.01 in the calculation of the curve in Fig. 2 due to an uncertainty of ±150 G in the value of the magnetic field at the pole tips of the sextupole magnet. Within the ionization region, there is no significant variation of s as a function of axial position.

The factor f(H) in Eq. (6) is the hyperfine structure (hfs) coupling function 26) and is shown for ^{6}Li and ^{7}Li in Fig. 3. At zero field f(H) takes on the value $1/(2I + 1)$, in which I is the nuclear spin. In strong fields, where the

nuclear and electronic spins are decoupled, f(H) approaches unity. The electronic polarization of a beam consisting of an isotopic mixture is the weighted average of $P_{e,atom}$ calculated for each isotope separately. For the axial magnetic field dependence, H(z), shown in Fig. 4, the weighted average, $\bar{f}$, of the hfs coupling function, for the isotopic mixture of the Li beam used in PEGGY, varies from $\bar{f} = 0.93$ to $\bar{f} = 0.97$ over the length of the ionization region.

To obtain high electronic polarization in fields not larger than ~200 G, which is the limit imposed by emittance considerations, an alkali atom with a small hfs splitting is needed. Lithium 6 was chosen since it has a small hfs splitting of 228 MHz and a small nuclear spin value of I=1. Furthermore, the photoionization cross section of Li (see Fig. 5) is the largest of all the alkali atoms. In addition depolarizing effects due to spin-orbit coupling in continuum states are negligible in Li 26,65). Disadvantages in the use of lithium are its high boiling point, which dictates high temperature (~875°C) operation of the oven, and its short photoionization-threshold wavelength (230 nm), which necessitates the use of far-uv optics.

The polarized ^{6}Li atoms are photoionized by pulsed uv light, which is focused and directed onto the lithium atomic beam in the ionization region by an ellipsoidal mirror and a 45° plane mirror. An additional pass through the interac-

tion region is provided by a retro-reflector. The ionization region is maintained at a potential of -70 kV, and the photoelectrons are accelerated to ground potential during extraction. A repeller electrode prevents the electrons from leaving the ionization region in the backward direction. The lithium ions drift toward the surrounding electrode surfaces.

2.2 DEPOLARIZING EFFECTS

The polarization of the extracted electron beam is degraded from the value $P_{e,atom}$ if the beam contains unpolarized background electrons originating at the electrode surfaces by photoemission or field emission. This background contamination can be avoided by careful design of the electron-optical configuration. Intensity measurements with the atomic beam off demonstrated that the background electrons contributed $<10^{-3}$ to the beam intensity. In addition depolarizing effects during the extraction process were estimated to be negligible.

The photoionization of any Li_2 molecules in the beam reduces the polarization. The degree of depolarization caused by the presence of Li_2 in the atomic beam is given by the product of the fraction of Li_2 molecules in the beam at the ionization region and the ratio of the molecular to the atomic photoionization cross sections. For an oven tempera-

ture of 875°C and an orifice temperature of 925°C it can be shown 26,66) that the fraction, γ, of Li_2 in the beam at the oven orifice is 0.035. The value of γ at the ionization region, however, is substantially smaller since the Li_2 molecules are not focused by the sextupole magnet. The effective solid angle for transmission, Ω_m, of the Li_2 molecules from the oven to the ionization region is given simply by the geometric acceptance angle which in our case is $\sim 6 \times 10^{-5}$ sr. The effective solid angle for transmission of unpolarized atoms $\Omega_a = (\Omega^+ + \Omega^-)/2$, as calculated from the sextupole computer program 26,64), on the other hand, is $\sim 3 \times 10^{-4}$ sr. Thus the molecular fraction, γ', at the ionization region is given by $\gamma' = \gamma\Omega_m/\Omega_a \approx 0.007$. Above the Li photoionization threshold, the photoionization cross sections for Li and Li_2 are known to be of the same order of magnitude 67). At threshold, where the only accurate measurements have been made, the cross section for Li_2 is three times that for Li. (See Ref. 67.) Therefore we assume that the photoionization of Li_2 results in a depolarization of the electron beam of $(3 \pm 2)\ \gamma' = 0.02 \pm 0.01$.

If an intense, broadband flashlamp is used for the photoionization, a substantial fraction of the Li atoms in the ionization region will undergo a transition to the 2P state prior to ionization by the uv light. Since the photoionization cross section for 2P atoms is much higher than that for ground state atoms (see Fig. 5), this two-step photoioniza-

tion process will significantly increase the electron beam intensity. However, the electron polarization will be reduced 26,51,68). As shown in Fig. 6, unpolarized 2S-2P resonant light at 670.8 nm incident parallel to the magnetic field induces transitions to magnetic substates at the 2P level which consist of a mixture of pure spin states. The result is the introduction of a factor of $(5/9)^n$ in the atomic polarization for those atoms which have undergone n excitations prior to photoionization. This depolarizing effect was almost completely eliminated with the use of a uv interference filter which removed ~99% of the 670.8 nm resonance radiation, resulting in a depolarization of $\lesssim 1\%$ at high light intensity. This filter also reduced the uv light intensity by a factor of ~2. (See Fig. 7.)

2.3 POLARIZATION MEASUREMENTS

Two techniques were used to measure the PEGGY polarization. At 70 keV prior to injection, a Mott scattering polarimeter monitored the beam polarization, while at GeV energies a Møller scattering polarimeter was used.*

---

*High energy elastic scattering from a polarized proton target provided an additional check on the high energy polarization 1).

2.3.1 Mott scattering

The scattering of electrons at energies of ~100 keV by the electric field of heavy nuclei is a standard method 69-71) for determining the electron polarization, P_e. The measured quantity is a left-right scattering asymmetry, Δ_M, for a transversely polarized beam. The polarization and scattering asymmetry are related by $P_e = \Delta_M / S$ with $\Delta_M = (N_L - N_R)/(N_L + N_R)$, where $N_{L(R)}$ denotes the left (right) counting rate, and the asymmetry function, S, is the analyzing power (Sherman function) of the scattering process. Calculations 72) give a value of ~0.4 for S if the electrons have a velocity of $v \sim 0.5\ c$ and are scattered from high Z nuclei into backward angles of $\sim 120^{\circ}$.

Although the Mott scattering method is simple in principle, corrections have to be applied to the measured asymmetry for instrumental efficiencies, detector acceptances, multiple and plural scattering events within the foil, and various background contributions 26). If the counting rates N_L and N_R are measured simultaneously by two detectors symmetrically placed relative to the incident beam, the measurement of Δ_M will be insensitive to beam intensity fluctuations. Exchanging the detectors by a rotation of 180° around the beam axis provides a means for normalizing instrumental efficiencies and detector acceptances if care is taken to avoid the introduction of a new asymmetry by this

rotation. With the use of several scattering foils of different thicknesses, the effect of multiple and plural scattering events can be determined to provide a calibration of the Mott polarimeter for any one of the foils. Beam dependent background effects, such as inelastic scattering from the foil or chamber walls, which do not give rise to a left-right asymmetry, can be taken into account with the use of energy-sensitive detectors and pulse height analysis.

For a polarization analyzing system which employs counting techniques, a relatively low beam intensity is needed. Since a spin rotation from the initial longitudinal direction to a transverse direction is also required, 90^{o} scattering from a gold foil (prior to the 120^{o} analysis scattering) can be used to satisfy both requirements. The rotation of the polarization vector during the 90^{o} scattering is small and calculable.

2.3.2 Møller scattering

Elastic electron-electron (Møller) scattering has been extensively employed at energies of ~1 MeV 69,73) to measure electron polarization. This technique was chosen as the means to determine the high energy beam polarization at SLAC because the cross section and analyzing power are large and the process is purely quantum electrodynamic. The Møller asymmetry and laboratory cross section at the representative

incident beam energy of 9.712 GeV are shown in Fig. 8. A Møller target consists of a thin ferromagnetic foil magnetized to saturation in an axial magnetic field and inclined at a small angle with respect to the beam direction to provide a large component of longitudinal polarization. Reversal of the field direction reverses the polarization of the target. The asymmetry in the scattering can then be measured in a single arm experiment by periodically reversing either the beam or target polarization 23). The scattered electrons, after separation from the primary beam by a bending magnet, are analyzed in momentum and scattering angle by a spectrometer containing appropriate detection and particle identification elements.

SECTION 3

APPARATUS

3.1 GENERAL LAYOUT

Top and elevation views of the installation of the polarized electron source at SLAC are shown in Fig. 9. PEGGY was located in the beam line tunnel of the linac but separated from the injector by a radiation wall which permitted source maintenance during accelerator operation. An achromatic beam transport system carried the polarized electrons from the source through the radiation wall into the injector.

PEGGY consisted of four major components: an oven chamber, an ionization chamber, an optics chamber, and a Mott scattering chamber. Inside the oven chamber, shown schematically in Fig. 10, were the atomic beam forming elements comprising the Li oven, collimators, beam chopper, and sextupole magnet. The ionization chamber, also shown in Fig. 10, housed the electron-optical elements required for extraction of the photoelectrons as well as the 45^{o} plane mirror and a spherical retro-reflector which redirected the light onto the lithium beam with maximum overlap. Immediately below the ionization chamber was the optics housing containing the uv flashlamp and the ellipsoidal mirror which focused the uv radiation onto the ionization region.

As shown in Fig. 9, a 14^{o} bend was located downstream from the ionization region. A pulsed magnet at this bend was used to direct the electron beam either into the transport line for injection into the accelerator or into the Mott scattering chamber for polarization analysis.

In the following parts of this section we will present a detailed discussion of the various components of the apparatus.

3.2 ATOMIC BEAM

To produce an atomic beam with the required intensity and running time, a suitable lithium oven had to be developed. Significant atomic beam intensities can be achieved only with Li vapor pressures of several Torr within the oven, corresponding to oven temperatures well above $750^{o}C$. At these high temperatures, the corrosive effects of Li are substantial, with the consequence that containment materials generally must be restricted to low carbon steels and several refractory materials 74). Thus, the oven body, shown in Fig. 11, was fabricated from ARMCO (ingot) iron; in order to eliminate welded joints in contact with liquid Li metal, the oven body was machined from a solid block. The oven top, which included the Li filling port, and the oven orifice were machined from type 430 stainless steel (a ferritic steel). Since past experience had shown that inert gas

tungsten-arc welded joints became porous after extended exposure to hot Li vapor, the oven parts were joined by electron beam welding with a 1 cm deep penetration weld.

In order to permit high temperature operation, the oven was thermally isolated from its surroundings with three tungsten pins used for support and four layers of stainless steel sheet used for a heat shield. The walls of the oven chamber and a copper box surrounding the heat shield were cooled with freon. To maintain the oven at an operating temperature of 875°C, ~600 W of heating power were required. The heating power was provided by ~35 m of Thermocoax* type 1 Nc I 20 resistive heating cable wound around the oven. Separate windings permitted the oven top and orifice to be operated at higher temperatures than the oven bottom, a condition necessary for stable operation. The oven temperatures were monitored with three chromel-alumel Thermocoax* type 2 AB I 20 thermocouples at the oven bottom, top, and orifice respectively. Two ovens constructed in this manner have been successfully operated at high temperature for more than 500 hours each with no noticeable deterioration. Two smaller ovens, similarly constructed but with only 1/4 of the lithium capacity, have also been operated for extensive periods of time (>1000 hours each) with little noticeable deterioration.

---

*Amperex Electron Corporation, Hicksville, NY 11802.

In the design of the atomic beam, a conventional type beam from a large bore orifice was adopted. Dimensions of the atomic beam forming system are shown in Fig. 12. The exit orifice of the oven had a radius, a_0, of 0.85 mm and a channel length of ~1.2 mm. For pure effusive flow sources the mean free path, λ_0, of the particles in the oven must be greater than either the radius or the channel length of the exit orifice. If these conditions are met, then the number of atoms emerging per second into a solid angle $d\Omega$ at an angle θ with respect to the normal to the exit orifice is given 75) by

$$N(\theta)\, d\Omega = 1.1 \times 10^{22}\, p_0 A_0 (MT_0)^{-1/2} \cos\theta\, d\Omega \text{ atoms } s^{-1} \qquad (8)$$

where p_0 is the oven pressure in Torr, A_0 is the area of the exit orifice in cm^2, M is the molecular weight, and T_0 is the oven temperature in K. Thus for effusive flow conditions, the number of atoms emitted per second is proportional to $p_0 T_0^{-1/2}$.

If $\delta = 3.1 \times 10^{-8}$ cm is the effective diameter of a Li atom as determined by viscosity and diffusion measurements 76), then λ_0 for Li is given by*

---

*No measurement of the appropriate mean free path of Li atoms exists. A discussion of the suitability of using the diameter as determined by viscosity or diffusion measurements for calculating mean free paths is given in Refs. 75) and 77).

$$\lambda_0 = 2.4 \times 10^{-19} T_0 p_0^{-1} \delta^{-2} = 2.5 \times 10^{-4} T_0 p_0^{-1} \text{ mm} . \quad (9)$$

Consequently, for our operating conditions ($T_0 \gtrsim 1150$ K, $p_0 \gtrsim 7.8$ Torr), the mean free path predicted by Eq. (9) was $\lesssim 0.04$ mm. Thus since the ratio λ_0/a_0 was $\lesssim 0.05$, the flow through the exit orifice was in the transition range between pure viscous flow for which $\lambda_0/a_0 < 0.01$ and pure effusive (molecular) flow 78) for which $\lambda_0/a_0 > 1$.

It is expected that particle-particle scattering in the vicinity of the exit orifice should reduce the beam intensity in the forward direction relative to that predicted for pure effusive flow 75). The first collimating aperture (see Fig. 12), which was placed ~2.5 cm in front of the oven orifice, shortened the axial distance along which particle-particle scattering could occur, but introduced additional particles backscattered from the collimator structure. This backscattering was reduced by maintaining the collimator at a temperature of ~400°C, which was warm enough to avoid build-up of Li in the collimator aperture, and cool enough to permit most of the lithium atoms striking the collimator structure to condense and flow away from the aperture into a removable Li recovery bottle located below the collimator. If the pumping speed between the oven and first collimator is sufficiently high, the mean free path will increase rapidly as the atoms move away from the oven orifice. In fact, as shown in Fig. 13, the atomic beam intensity measured at a surface-ionization detector located downstream from the sex-

tupole magnet showed no significant deviation from effusive flow predictions until the source temperature exceeded 875°C.

Occasionally, lithium condensed at the aperture of the first collimator forming a "clog" which blocked the beam. Generally, these clogs were removed and normal atomic beam intensities restored within 1 h by temporary heating of the collimator to a temperature of ~600°C. (It was found that fewer clogs formed when the surface of the collimator was left unburnished after cleaning with deionized water and ethanol.)

In order to minimize buildup of Li in the sextupole magnet, a second collimator was placed in front of the magnet entrance. In addition, a mechanical chopper in the form of a thin rotating disk with 6 holes on the circumference having a total transmission of 6%, was placed between the two collimators. The angular velocity and phase of the chopper were synchronized with the flashlamp trigger pattern such that the atomic beam in the ionization region was at its full intensity during the light pulse. Normally, the second collimator was operated at a slightly higher than ambient temperature. For a few minutes every 12 hours, however, its temperature was raised to about 275°C to permit accumulated Li to drain off. (Higher temperature operation was precluded by the proximity of the sextupole magnet.)

During the course of PEGGY's development, two sextupole magnet designs have been used. Scale drawings of the cross sections of these permanent magnets are shown in Figs. 14 and 15; the significant magnet parameters are listed in Table II. The small bore magnet,* which was used in the early stages of development, had a state selection parameter, s, very close to unity. Since computer calculations** indicated that a substantial increase in beam intensity with only a minor reduction in polarization could be achieved with a larger bore magnet, such a magnet was constructed at SLAC and has been used exclusively since 1975. According to the computer calculations, the effective solid angle, Ω^+, for transmission of $m_J = + 1/2$ atoms through the large bore magnet is almost a factor of 2 larger than that for the small bore magnet. However, the $m_J = - 1/2$ solid angle, Ω^-, for the large bore magnet is 10 times that for the small bore. Nonetheless, for the large bore magnet, Ω^- is still small compared to Ω^+ so that s is reduced by only ~2%.

The atomic beam forming components were aligned with respect to the optical axis with the aid of a telescope and a small 45° plane mirror located near the Mott chamber. During operation of PEGGY, the collimator apertures and the

---

*Fabricated by Frequency and Time Systems, Inc., Danvers, MA 01923.

**The computer calculations are described in Refs. 26) and 64).

oven orifice could be viewed with the telescope (the second collimator could be illuminated by a filament which was located between the two collimators just out of the beam path). The horizontal and vertical positions of both the oven and the first collimator were adjustable from outside the vacuum system.

The atomic beam intensity was monitored 36 cm downstream from the center of the ionization region by an adjustable surface-ionization (Langmuir-Taylor) detector 79,80) consisting of an oxidized and heated tungsten wire 0.13 mm in diameter and 1.25 cm in length. The profile of the atomic beam produced at an oven temperature of 875^{o}C, transmitted by the large-bore sextupole magnet, and measured by the surface-ionization detector is shown in Fig. 16a together with the calculated profile from the computer analysis. As can be seen the agreement is good, except in the wings of the profile. The calculated profile at the center of the ionization region, shown in Fig. 16b, indicates that the full width half maximum of the atomic beam was 0.30 cm. Calculations also show that for an oven temperature of 875^{o}C (for which the mean velocity in the atomic beam is $\sim 2 \times 10^{5}$ cm/sec), the atom density on axis at the ionization region was 3×10^{11} atoms/cm^{3}, and that for a cylindrical ionization volume measuring ~0.6 cm in diameter by ~4 cm long there were $\sim 10^{11}$ atoms available for ionization.

The maximum capacity of the large oven was 750 g Li. At the normal operating oven temperature of 875°C, a full intensity running time of ~175 h was possible before the oven charge was depleted. In order to reload the system, the empty oven was allowed to cool, after which the oven chamber was backfilled with Ar and the components were removed. Deionized water and ethanol were used to clean lithium and lithium compounds from the oven chamber walls and the components. A second set of previously cleaned components--including an oven already filled with Li--was installed and the oven chamber was baked for 6 h (with the chamber walls at ~150°C and the oven at ~320°C) before the oven was heated to its normal operating temperature.

Because of the vacuum requirements of the accelerator, only oil-free pumps were used for evacuation. For this reason, a bellows pump was used to rough the system to ~1/9 atm, after which sorption pumps were used to provide a vacuum of $\sim 10^{-2}$ Torr during the baking of the oven chamber. For oven temperatures exceeding 320°C, a high vacuum was necessary to avoid contamination of the lithium and to eliminate any attenuation of the atomic beam by residual gas scattering. A vacuum of 10^{-6} Torr was maintained by a 600 ℓ/s ion pump located directly below the oven chamber. In order to prevent the ion pump from stalling, a minimum of 10 h was required to raise the oven temperature from 320°C to the normal operating value of 875°C.

Oil-free Li consisting of 95.6% ^{6}Li and 4.4% ^{7}Li sealed in metal cans under an Ar atmosphere was obtained from Oak Ridge National Laboratory.* All Li handling was done under an Ar atmosphere in a glove box which surrounded the access flange of a separate vacuum chamber used for melting the Li into the oven. To fill an oven, Li was placed in a funnel which was inserted into the oven filling port. The oven, funnel and Li were then heated to ~250°C in a vacuum of ~10^{-2} Torr until the Li melted and flowed into the oven. The original "skin" of the Li, which often had a dull gray-white appearance, remained behind in the funnel.

By removing the Li recovery bottle from the oven chamber, mounting it upside down on top of the Li melting chamber, and heating the bottle until the Li flowed into the funnel below, approximately 2/3 of the Li from any oven charge could be recycled. After filling, the oven was cooled and stored in the Li melting chamber under an Ar atmosphere until needed. The Li filling port was sealed prior to removing the oven from the glove box. Exposure of the Li to air was thus limited to the air which entered the oven through the orifice during the ~30 minutes required to install and begin the evacuation of the oven in the PEGGY vacuum system.**

---

*Oak Ridge National Laboratory, Isotope Sales Department, Oak Ridge, TN 37830.

**In spite of the extensive precautions taken to minimize contamination of the Li, a clog of the oven orifice occurred occasionally which could not be removed by extended

3.3 LIGHT SOURCE AND OPTICAL SYSTEM

The light for photoionization of the lithium atoms was provided by a flashlamp. The components of the optical system used for transferring the light to the ionization region, shown in Fig. 10, consisted of a primary focusing mirror, uv interference filter, optics housing, vacuum window, 45° plane mirror and retro-reflector mirror. The photoionization cross section for Li, as determined by several authors, is shown in Fig. 5. As can be seen from the figure, the cross section for ionization of ground state Li remains high well into the vacuum ultraviolet region. To utilize a broad spectral range, the optical system was designed for maximum efficiency in the wavelength range 170 nm - 230 nm; that is, from the cutoff in transmission of quartz to the threshold of ionization of ground state Li.

3.3.1 Flashlamp

The successful development of the polarized electron source depended on the availability of a pulsed uv flashlamp of high intensity and brightness. The lamp had to be able to operate at the accelerator repetition rate of 180 Hz with

---

superheating of the orifice to 1020°C. Inspection usually showed that the orifice was completely covered by a brittle film. Spectroscopic analysis of a film sample revealed that the major non-lithium component was carbon. In some rejected shipments of Li, carbon inclusions of up to 5 mm diameter were found.

a pulse width of ~1.6 μs. In addition, good arc stability and lamp lifetimes of at least 10^7 pulses were required. The sealed xenon flashlamp initially used was replaced in 1975 with a vortex stablilized argon flashlamp.

The design of the sealed flashlamp was developed by a Yale collaboration with the Naval Research Laboratory 81). The final design,* shown in Fig. 17, consisted of sintered tungsten electrodes separated by a 4 mm gap. The lamp had a Suprasil quartz envelope (minimum distance to gap ~2 cm), and was filled with 5 atm Xe to optimize light intensity and lamp lifetime. The useful lifetime of ~3×10^6 pulses (determined by a 50% decrease in light output) was limited by deposition of tungsten on the lamp envelope.

The measured intensity distribution varied approximately with the cosine of the angle on either side of the median plane. The arc channel, while relatively fixed at the pointed anode, wandered about the axis of the cathode by as much as 2 mm. Consequently, the pulse to pulse variation of the overlap of the arc image with the atomic beam in the ionization region resulted in a fluctuation of the photoelectron yield of ~20%.

---

*Model L-1841 manufactured by ILC Technology, Inc., Sunnyvale, CA 94086.

To increase the light intensity and lamp lifetime, and to improve the pulse to pulse stability, a vortex stablized flashlamp of the type first developed by Mack 82) was designed and constructed 83) at SLAC. To form a vortex, the fill gas was admitted under pressure through tangential jets located at the cathode side of the lamp and exhausted through an axial hole in the cathode and through an annular opening around the anode rod, as shown in Fig. 18. The axial angular momentum imparted to the gas formed a radial pressure gradient which served to stabilize the location of the arc channel to ~±0.1 mm. The gas flow also carried away material sputtered from the electrodes, greatly reducing the deposition rate on the lamp envelope. The anode was a 3 mm diameter solid thoriated-tungsten (98% W, 2% Th) rod with a flat face. The tungsten (2% Th) cathode rod had a 9.5 mm diameter which tapered to a flat face 5.1 mm in diameter. The anode-cathode gap was 10 mm. Lamp performance was found to improve when the lamp inlet gas pressure was increased to ~5 atm, the limit of the gas compressor. The argon gas, which was recirculated at a flow rate of ~ 4.5 ℓ/s STP, was extensively filtered to remove organic contaminants introduced by the gas compressor. Periodic monitoring of the recirculated argon indicated that the gas contained less than 5 ppm of oxygen or water vapor.

The light output in the useful spectral range of 170-230 nm had a value of ~0.5 J per pulse for a lamp current pulse

of 7.0 kA peak. The lamp could be operated for at least $\sim 2 \times 10^7$ pulses (31 h at 180 pps) with only a small decrease in the uv intensity and with a pulse to pulse variation in intensity of $\lesssim 5\%$. Slight darkening of the lamp envelope and consequent deterioration of light intensity was apparent after this time. The lamp was rejuvenated easily with the replacement of the Suprasil envelope* and the reworking of the surfaces of both electrodes which became eroded and discolored in use. To facilitate rapid lamp replacement, two interchangeable lamp mounts were constructed. A lamp could be removed from the optics housing and replaced by the spare within ~30 minutes.

The vortex-stabilized flashlamp was a considerable improvement over the sealed flashlamp in intensity, lifetime and positional stability of the arc. A typical arc pattern of the vortex-stabilized lamp is shown in Fig. 19. Typical spectra for both lamps are shown in Figs. 20 and 21. These spectra were measured with a portable Bausch and Lomb monochromator and ITT photodiodes of known spectral efficiencies.** An overall normalization determined at several wavelength regions using selective filters of known

---

*The 30 mm o.d. by 1.5 mm wall Suprasil tubing was supplied by Heraeus-Amersil, Inc., Sayreville, NJ 08872.

**The photodiodes were calibrated in the laboratory of W. E. Spicer, Stanford University, by comparing their spectral sensitivity to standards provided by the U.S. National Bureau of Standards.

transmission was applied to the final curves to correct for variations in monochromator efficiency and solid angle acceptances.

The current pulse for the flashlamp was generated by a thyratron-switched modulator (Fig. 22) which was a standard SLAC klystron modulator 84) modified for higher current and voltage capabilities. A 20 kV dc high voltage supply charged the capacitors in the pulse forming network (PFN) through a resonant charging circuit to a maximum of 40 kV. The trigger input was amplified and applied to the control grid of a high current hydrogen thyratron switch tube. When the switch became conducting, the charge stored on the PFN capacitors was dissipated in the lamp arc and the 2Ω load resistor. The modulator could provide a current pulse of 1.6 μs duration of up to 8 kA into a resistive load of 2Ω at repetition rates up to 180 pps. To produce a peak lamp current of 7.0 kA, the PFN capacitors were charged to 33.6 kV. The integral of the spectrum shown in Fig. 21 between 170 and 700 nm, into 4π steradians, represents about 1.5% of the energy stored in the PFN. A typical light intensity pulse along with the corresponding lamp current pulse is shown in Fig. 23.

3.3.2 Mirrors

An ellipsoidal mirror was used as the primary focusing mirror to concentrate the uv light in the ionization region. The flashlamp was centered at the inner focus and the ionization region, as reflected in the 45° plane mirror, at the other focus. The semimajor and semiminor axes of the ellipsoid were 35.5 and 27.3 cm respectively. The mirror surface was an annular segment of the ellipsoid. The mirror, shown in Fig. 18 together with the vortex lamp, subtended a solid angle of 4.7 and 0.4 sr as seen from the inner and outer foci respectively. The magnification of an image formed at the outer focus was ~3.5 in the transverse dimension and ~10 in the longitudinal direction. Thus the image of the arc pattern shown in Fig. 19 had a diameter of ~0.75 cm at the outer focus of the ellipsoidal mirror.

The primary focusing mirror blank was machined from aluminum to an accuracy of ~0.02 mm of the ellipsoidal form. The surface was then plated with Kanigen (electroless nickel) which served as a substrate for optical polishing.* The final ellipsoidal form of the mirror was such that a point light source placed at the inner focus produced an

---

*The polishing was carried out by the Electro-Optical Division of the Perkin-Elmer Corp., Norwalk, CT 06856. Scattered light due to surface roughness was specified to be no more than 1% at 632.8 nm. The percentage of uv light scattered would be expected to be greater.

"image" at the outer focus less than 1.0 mm in diameter. To achieve maximum reflectance in the uv, the mirror was aluminized and overcoated with MgF_2.* The measured reflectance is shown in Fig. 7. Care was taken at all times to keep the mirror stored in a clean, dry atmosphere since MgF_2 is hygroscopic and since small amounts of organic vapors deposited on the mirror surface could adversely affect performance.

The 45^{o} plane mirror, located inside the vacuum chamber, reflected the converging light cone onto a horizontal axis, achieving maximum overlap with the atomic beam in the ionization region. This mirror was a polished quartz disk 24 cm in diameter and 0.6 cm thick, the front surface of which was aluminized and overcoated with MgF_2 for maximum reflectance in the uv as in the case of the ellipsoidal mirror. The measured reflectance is shown in Fig. 7. A 1.3 cm diameter hole machined through the mirror at 45^{o} allowed the atomic beam to enter the ionization region, as shown in Fig. 10. Although the mirror was maintained at a temperature of 200^{o}C to avoid deposition of Li scattered from the atomic beam, it gradually became cloudy and degraded in performance and after several months of operation had to be replaced.

After its first passage, the light was reflected back into the ionization region by a 13 cm diameter spherical

---

*The mirror was coated by Acton Research Corp., Acton, MA 01720.

mirror with a radius of curvature of 14 cm. This second passage of light contributed 10-20% to the photoelectron yield. The spherical retro-reflector was fabricated from stainless steel and, as in the case of the ellipsoidal mirror, its optical surface was aluminized and overcoated with MgF_2. A Suprasil quartz disk placed over the reflecting surface protected the coating from scattered Li, while a 90% transparent wire mesh placed in front of the quartz disk served as the ground plane for the extraction field. A 3 cm diameter hole through the center of the retro-reflector assembly allowed extraction of the photoelectrons from the ionization region, as shown in Fig. 4.

3.3.3 Filter

As its spectrum reveals, the SLAC vortex lamp produces intense red as well as uv light. Since excitation of Li by the resonant 2S-2P line at 670.8 nm decreases the atomic electronic polarization (see Section 2.2), the red light was removed by a broadband uv interference filter* introduced into the light cone just above the flashlamp. The filter consisted of a Suprasil grade quartz disk coated with alternating layers of MgF_2 and Al forming the interference cavity. Precise control of the uniformity and thickness of the films was required to achieve the large bandwidth and high transmission shown for this filter in Fig. 7.

*Developed by Acton Research Corporation, Acton, MA 01720.

3.3.4 Optics Housing

A sealed housing enclosed that part of the light path which lay outside the vacuum system. Oxygen absorption of the uv light below 185 nm was eliminated by replacing the ordinary atmosphere in the housing with dry N_2 gas, resulting in a 20% increase in photoelectron yield. The controlled atmosphere also served to protect the primary mirror, interference filter and vacuum window from organic vapors which would be cracked by the uv light, forming harmful deposits on these surfaces. Ozone, which otherwise would be present in unhealthful amounts, was also eliminated by the use of an N_2 atmosphere.

The lower plate of the optics housing served as the support for a motion assembly upon which the primary focusing mirror was mounted. Couplings through the housing wall allowed external positioning of the mirror with five degrees of freedom. Attached to the optics housing was a vertical lift mechanism which facilitated lamp changes. A window on the side of the housing at the level of the flashlamp arc allowed the light intensity to be monitored by a photodiode.

3.3.5 Vacuum Window

A 28 cm diameter by 2.0 cm thick polished Suprasil disk served as vacuum window for the light. The measured transmission of the window is shown in Fig. 7.

3.4 ELECTRON EXTRACTION AND TRANSPORT

The ionization region is a cylindrical volume approximately 4 cm in length and 0.6 cm in diameter and essentially is defined as the volume within which those photoelectrons accelerated to high energy originate. The extraction efficiency for all photoelectrons originating in this volume is believed to be close to unity. This region was centered on the axis of the atomic beam at the outer focus of the ellipsoidal mirror, the center of which was ~28 cm downstream from the exit of the sextupole magnet. The boundaries of this region were established primarily by the restrictions imposed on the beam emittance and energy spread by the linac injector. An axial magnetic field of ~215 G was produced in the ionization region by a cylindrical coil (5.8 cm mean diameter) which was mounted coaxially with the atomic beam but with its center 24 cm downstream from the ionization region. The dependence of the axial component of the magnetic field on axial positon is shown in Fig. 4. The direction of the magnetic field and thus of the electron polarization could be reversed in $\lesssim$1 sec by reversing the current through the cylindrical coil.

The ionization region was surrounded by axially symmetric electrodes, as shown in Fig. 4, which served to extract the photoelectrons and form them into an electron beam. The cathode, biased at -70 kV, defined the mean energy of the

electron beam. The repeller electrode prevented photoelectrons from leaving the ionization region in the backward direction. The repeller potential, which was -77 kV, introduced an axial electric field of ~350 V/cm over the length of the ionization region. Thus the maximum value of ΔE = 1.5 kV for the full width half maximum energy spread accepted by the linac injector (see Section 1.1) placed an upper limit of ~4 cm on the length of the ionization region. The axial electric field was strong enough to overcome any influence of space charge effects during extraction. The main acceleration of the beam to its 70 keV mean energy occurred in the gap between the cathode and the grounded anode. On the upstream side the repeller electrode was surrounded by a grounded shield which controlled the potential in that region and eliminated possible disturbing influences on the electron optics by the accumulation of charge on the vacuum window and the 45° plane mirror. This shield also prevented uv light from striking the repeller and cathode, thereby releasing unwanted background electrons. Representative trajectories of photoelectrons created in the ionization region as well as on electrode surfaces are shown in Fig. 4, together with the potential profile produced by the electrodes.* As can be seen, background (surface) photoelectrons were spatially well separated from the atomic beam

---

*The trajectories were calculated with the SLAC Electron Trajectory Program 85).

photoelectrons and were easily eliminated from the electron beam by the electron transport system further downstream from the ionization chamber.

All electrodes were fabricated from stainless steel. They were designed with rounded edges and polished consistent with standard high voltage practice. The electrodes were mounted on a machinable ceramic structure* which had grooves cut into its surface to suppress possible surface discharges. The repeller and cathode potential leads from a 100 kV, 3-pin feedthrough** were insulated with glass tubing to prevent breakdown.

The electron beam transport system was designed for a source emittance matched to the acceptance of the linac injector. For an axial magnetic field of H = 215 G at the center of the ionization region and for values of v' and v corresponding to 70 keV and 1 eV respectively, Eq. (5) gives a generalized emittance of $\varepsilon^* \sim 10$ mrad-cm if ρ is assumed to be 0.3 cm. Since the radius of the image of the lamp arc at the ionization region was about 0.37 cm (Section 3.3), and since the halfwidth of the atomic beam profile at 20% of the maximum intensity was ~0.3 cm (see Fig. 16b), ρ could not have been appreciably larger than 0.3 cm. On the other

---

*Aremcolox Grade 502-400, manufactured by Aremco Products, Inc., Briar Clift Manor, NY 10510.
**Type 809C5358, manufactured by Ceramaseal, Inc., New Lebanon Center, NY 12126.

hand, since the transmission of the PEGGY beam through the injector was clearly less than unity (the observed values averaged ~2/3), and if this decrease from unity is attributed to the influence of the radial extent of the source region on the emittance, then ρ could not have been much smaller than 0.3 cm. Consequently the radius of the ionization region is taken to be $\rho = 0.30 \pm 0.15$ cm. (The variations of the axial magnetic field and beam velocity in the ionization region do not significantly affect the uncertainty in ρ.)

The beam was transported through a 5 cm diameter tube a distance of about 7 m from the ionization region to the linac injector as shown in Fig. 9. During transport, the beam was confined by a periodic array of thin solenoidal magnet lenses spaced at approximately 1 m intervals. The betatron phase shift per period was 90°; that is, each lens imaged from the previous lens to the following lens. The gross effects of stray magnetic fields were cancelled with large compensating coils surrounding the entire source and the first 4 m of the beam transport system. To compensate for small misalignments and residual stray magnetic fields, steering coils were placed adjacent to each lens. The final balance of the electron beam intensities for the two electron helicities was accomplished by having independent control of the first few steering coils for each of the two beam helicities. When the helicity was reversed these coils

were switched to a second set of power supplies and simultaneously the axial direction of the magnetic field in the first few lenses was reversed.

PEGGY was installed with its axis parallel to, but horizonally offset from, the accelerator axis by a distance of 90 cm, in order to prevent the Li atoms from entering the accelerator and to facilitate efficient radiation shielding by traversing a shielding wall at an angle. The electron beam was guided through this offset by two identical 14^{o} air-core bending-magnets excited in series and placed one betatron wavelength apart. Since the second bend was in the opposite direction to the first, the dispersion effect of the first was cancelled provided the plane of dispersion had no net rotation produced by the lenses between them. Because a solenoid rotates the beam and hence the plane of dispersion, it was necessary to arrange the lens strengths and polarities so that the net rotation was zero; that is, so that $\int B\, dz$ vanished between the two bends. In order to achieve this condition, the beam was transported between the two bends by three lenses, the first and third of which were operated in series with field directions opposed, while the middle lens was constructed of two identical lenses mounted together with their fields in opposition so that this middle lens assembly was irrotational by itself. Thus the offset was achromatic (independent of energy) to first order, a condition required to accommodate a 2% spread in the beam

energy. (Nonzero second order terms remained because the lens focal length and hence the betatron wavelength depended on energy.)

A freon-cooled baffle was installed at the first 14^{o} bend in order to trap any Li atoms which might scatter past the first bend. Two silicon wafers were located downstream from the cold trap to monitor possible Li contamination. The wafers were periodically removed during accelerator down-times and examined for evidence of Li by Auger-spectroscopic surface-analysis techniques. An rf cavity located in the injector and excited to high rf electric fields provided a Li monitor during accelerator operations. As a safety feature, a fast valve which was located between the source and the accelerator injector as shown in Fig. 9, was interlocked to the source pressure gauges. Any malfunction in the source resulting in a very rapid rise in pressure would cause the fast valve to close, preventing a pressure shock from entering the accelerator. Likewise, a slow pressure rise above a preset value would cause two slow valves to close, isolating the source from the accelerator. Detection of electric field breakdowns in the rf cavity or failure of the rf power supply would also cause the slow valves to close.

In order to optimize the settings of the lens and steering coils, beam intensity monitors were installed at several

locations along the transport tube. The first monitor was a Faraday cup with a downstream endflap that could be opened or closed under vacuum. Since the endflap had to be closed during a measurement, the Faraday cup did not provide a continuous beam monitor. Noninterrupting current measurements were made with toroids placed before and after each of the two 14° bends. Additional beam monitors shared by the normal unpolarized SLAC gun beam were located in the injector section. Preliminary tuning of the PEGGY beam was facilitated by the use of a stainless steel mesh which could be inserted into the ionization region while the system was under vacuum. The electron beam intensity produced by photoemission from this mesh was typically two orders of magnitude larger than that of the polarized beam. Although the phase space of the two beams differed slightly, the mesh beam provided an effective means for determining the initial settings of the electron optical elements.

The first 14° air-core magnet was operated in a pulsed mode so that individual beam pulses could be transported selectively either to the injector or straight ahead to the Mott chamber for online polarization monitoring. The Mott transport line, equipped with its own steering and focusing coils, had a small vertical parallel offset near the entrance to the Mott chamber, as shown in the elevation of Fig. 9. The offset prevented Li from being deposited on the Mott scattering foils, kept uv light out of the Mott cham-

ber, and permitted a 45° plane viewing mirror to be mounted on the atomic beam axis, so that beam components could be aligned optically with the aid of a side mounted telescope.

3.5 MOTT SCATTERING

The arrangement used in PEGGY to measure the longitudinal beam polarization at low energy is shown in Fig. 24. The primary beam was first scattered from a thin gold foil mounted on target wheel $\mathcal{A}$. A series of collimators was then used to form the electrons scattered under 90° into a secondary beam. The transverse polarization, P_e^t, of this secondary beam is nearly equal in magnitude to the original longitudinal polarization. To measure the transverse polarization, the secondary beam was scattered from a second thin gold foil which was mounted on target wheel $\mathcal{B}$. Electrons back-scattered by 120° were detected with two Si surface-barrier detectors which were placed 180° apart in azimuthal angle in a vertical plane oriented perpendicular to the incident horizontal beam. Several gold foils of different thicknesses were mounted on target wheel $\mathcal{A}$ (299, 154, and 79 $\mu g\ cm^{-2}$) as well as on target wheel $\mathcal{B}$ (79, 39, and 24 $\mu g\ cm^{-2}$). Each target foil could be brought into position by rotation under vacuum. This rotation allowed an adjustment of the scattering rate with wheel $\mathcal{A}$ and an extrapolation of the asymmetries to zero foil-thickness with wheel $\mathcal{B}$.

The collimation of the scattered beam was such that only a small central part (~ 1/20) of the second-foil area was illuminated, whereas the size of the collimators in front of the detectors allowed each point on the detecting surface of 8 mm diameter to view fully a central portion of 1/3 of the foil area. Thus a dependence of the measured asymmetries on the intensity distribution across the scattered beam, which might change with the steering and focusing conditions, was avoided. For determining instrumental asymmetries, the detector positions could be reversed under vacuum by a rotation of 180° around an axis which coincided with the center line of the secondary beam path.

Several measures had to be taken to achieve a clean spectrum of the elastic double-scattering events, since the ratio of the incident rate to the double scattered rate was about 10^{10}. Relatively large ports (10 cm diameter) located downstream from the primary and secondary scattering foils, served as beam dumps for the fraction of electrons scattered in the forward direction by the foils. The stainless steel vacuum chamber had linear dimensions of about 30 cm and was lined on the inside with aluminum sheets in order to suppress the number of elastic electrons scattered from the chamber walls. Additional aluminum sheets divided the chamber into two parts each containing a target wheel. With crinkled aluminum foil blocking all slots between the sheets, the leakage of wall-scattered electrons to the area

of target wheel $\mathcal{B}$ was effectively reduced. In addition, the wall area which could be seen directly from the detectors (through the thin gold foil) was coated with carbon which served to further suppress the elastic background.

To permit measurement of backgrounds and to facilitate alignment and testing, an aluminum foil (675 μg cm^{-2}), a ZnS fluorescent screen, and an empty foil frame were mounted on target wheel $\mathcal{A}$, in addition to the three gold foils. Target wheel $\mathcal{B}$ on the other hand contained an aluminum foil (675 μg cm^{-2}), an open radioactive internal conversion source (^{109}Cd), and a bare Formvar backing, as well as the three gold foils. All gold foils had a diameter of 16 mm and were produced by vacuum deposition of gold onto Formvar films (~50 $\mu g/cm^2$) which had been stretched over frames consisting of thin aluminum rings 26).

For each detector the electronics for processing the signals consisted of a charge sensitive preamplifier, a pulse shaping amplifier and a linear time gate by which signals from various noise sources outside the time structure of the Mott pulses could be eliminated. After the time gate, the signals were routed either through a single channel analyzer to a dual counter or to a pulse height analyzer. Gating allowed the detector signals to be recorded separately for each direction of the beam polarization. The counters served as an approximate but direct indication of the polar-

ization. The pulse height spectrum was transferred to the data processing area where it was logged on magnetic tape for more precise polarization analysis.

Since PEGGY was operated at a constant pulse rate of 120 or 180 pps, Mott data were taken with the electron beam pulses which were not selected for acceleration to high energy. The steering and focusing elements used to transport the beam to the Mott scattering chamber were adjusted so that the beam was centered on the primary Au foil with similar shapes for both directions of the beam polarization.

A representative double-scattering electron spectrum is shown in Fig. 25. The counts within the elastic peak were first corrected for counts of inelastically scattered electrons. For the extrapolation of the inelastic background into the region of the elastic peak an exponential energy dependence was used. Typically, several percent of the counts within the elastic peak had to be subtracted for this kind of background. The counts were further corrected for elastic two-electron events which formed a resolvable peak in the pulse height distribution. Finally, as the Formvar backing was found to contribute to the elastic events as much as that of an equivalent 3 $\mu g\ cm^{-2}$ thick gold foil but with zero analyzing power, an equivalent fraction of counts was subtracted from the elastic totals. With the corrected number of counts within the elastic peak denoted by N_i^j for

detector i (i = 1 or 2) in position j (j = 0 or π) for both the forward and backward directions of the incident longitudinal beam polarization, instrumental asymmetries are eliminated if the Mott scattering asymmetry is calculated according to

$$\Delta_M = (\eta - 1)/(\eta + 1) \tag{10}$$

with

$$\eta = \left[(N_1^0 / N_2^0) / (N_2^\pi / N_1^\pi)\right]^{1/2} \tag{11}$$

The extrapolation of an asymmetry to its value at zero-foil thickness, $\Delta_M(0)$, is made according to

$$\Delta_M(t) = \Delta_M(0)\, e^{-\alpha t} \tag{12}$$

where t is the foil thickness and α the extrapolation constant. This constant was experimentally found to be $\alpha = 0.0044\ cm^2/\mu g$, which is in agreement with values in the literature for this scattering energy 86,87). Figure 26 shows one measurement of α, with Δ_M plotted for several foil thicknesses. The transverse polarization of the scattered beam is then given by

$$P_e^t = \Delta_M(0)/S \tag{13}$$

For an incident electron energy of 70 keV, extrapolation from tabulated values 72,88) gives S = 0.37 (±0.02) for the

range of scattering angles of $(120 \pm 4)^{o}$. The longitudinal polarization, P_e, of the incident electron beam is found from $\vec{P}_e^{\,t}$ by considering the change in the polarization vector caused by a 90^{o} single scattering event 89,90):

$$P_e^t = (1 - G/I)\, P_e \quad . \tag{14}$$

For 70 keV incident energy, the tabulated functions G and I 72,88) give $(1 - G/I) = 0.89$. The small fraction of plural and multiple scattering events within the foil can be shown 88,91) to give a negligible correction to Eq. (14).

3.6 ELECTRONIC INSTRUMENTATION

For high energy scattering experiments employing PEGGY, the helicity of the electron beam was reversed every 3 min under the control of the on-line computer at the high energy data processing area which was connected by a CAMAC serial link (twisted pair) to the PEGGY area. Furthermore, the relevant PEGGY operating parameters were monitored with the on-line computer by creating histograms from PEGGY information supplied over the CAMAC serial link by an analog multiplexer. Remote actuation of the PEGGY flashlamp, the 70 kV power supply, and the Li oven heaters was also possible via CAMAC. To facilitate the control of the PEGGY beam through the linac, a 10-channel, remotely selectable video link with a bandwidth of ~5 MHz provided a visual display of the source electron-beam pulse shape to the linac control center as well as to the data processing area.

SECTION 4

RESULTS AND DISCUSSION

Since its installation at SLAC in 1974, PEGGY has amassed more than 3000 hours in operating time. Modification of components, particularly the use of the larger bore sextupole magnet and the vortex stabilized flashlamp, and improvements in operating technique have led to an increase in the figure of merit, $P_e I_e^{1/2}$, by a factor of 4, and to substantially better long-term reliability of operation. The present operating characteristics of PEGGY are summarized in Table III.

4.1 INTENSITY

In its present configuration, with the uv filter in place, PEGGY is capable of producing an electron beam intensity averaged over a period of 2-3 h of 2.6×10^9 electrons/pulse at 70 keV, as shown in Table III. The intensity is subject to long term drifts resulting from gradual changes in both the atomic beam and flashlamp characteristics. Concommitant with the slight reduction in uv light intensity after $\sim 2 \times 10^7$ pulses of lamp operation, there is a gradual increase in the pulse to pulse intensity jitter which becomes excessive when the tip of the flashlamp anode

is worn away to the level of the anode flow separator (see Fig. 19). When the pulse to pulse jitter exceeded 5%, the flashlamp was replaced.

During the latest 1000 h of PEGGY operation, with the uv filter in place, the electron beam intensity at 70 keV averaged 2×10^9 electrons/pulse 92). Approximately 40% of this intensity was transported through the accelerator and was available for experiments at GeV energies. During running, the high-energy intensity was not allowed to exceed a maximum change of 5% when the polarity of the beam was reversed at the source. Fine tuning of the electron optics generally reduced this intensity difference upon reversal to ~2%.

4.2 POLARIZATION

The value of $P_{e,atom}$ calculated from Eq. (6) is 0.92 ± 0.04. When the depolarizing effects discussed in Section 2.2 are included, the predicted value* of the photoelectron polarization, P_e, is 0.89 ± 0.04.

As has been discussed in Sections 2.3 and 3.5, the polarization of the PEGGY beam was measured independently at the source energy of 70 keV by Mott scattering and at GeV ener-

---

*A slightly lower value, 0.847 ± 0.050, was given for the predicted value of P_e in Ref. 68) due in part to the use of too large a radius for the ionization volume in the computer calculation of the state selection parameter s.

gies by Møller scattering 23). With the uv filter in place, the Møller measurement provided a value of $P_e = 0.85 \pm 0.07$ 3,68), consistent with the predicted value of P_e and with the prediction that virtually no depolarization of the longitudinally polarized electron beam should result from the acceleration process. (See Appendix.) Mott scattering measurements provided a value of $P_e = 0.82 \pm 0.08$ after corrections for spin rotation in the primary foil and multiple and plural scattering effects in the secondary foil, as described in Section 3.5. Half of the uncertainty in the Mott measurement arises from non-statistical flucuations in P_e which are believed to be caused by changes in the portion of the electron beam sampled by the polarimeter. The remainder of the error includes the uncertainties in S, G, and the extrapolations in foil thickness and background events. The Mott value of P_e is consistent with both the Møller value and the predicted value. Small differences between Møller and Mott values are expected because the Mott polarimeter samples only a portion of the extracted beam. Since the acceptance of the Mott transport line is >10 mrad-cm, a larger radial extent of the ionization region is available for sampling. Based upon Fig. 2 it can be seen that deviations between Mott and Møller measurements of the order of ~0.05 are possible. Detailed comparisons of the Mott and Møller results at this level are precluded, however, by the present accuracies of the respective measurements.

4.3 AVAILABILITY

Central to the success of any experiment employing the PEGGY beam is the percentage of the time the source is available at full intensity. With the use of the larger (750 g capacity) oven, described in Section 3.2, the lifetime of an oven load was approximately 175 h. During the last three months of operation, the oven reloading time averaged about 43 h 92). Thus, with a lamp lifetime of ~31 h and with 1/2 h required for a lamp change, and with other downtimes, PEGGY's overall availability during the latest three months of operation exceeded 75%.

4.4 FUTURE DEVELOPMENTS AND APPLICATIONS

The operating characteristics described above indicate that PEGGY is eminently suited to experiments which require intensities of $\sim 10^9$ electrons/pulse and high polarization. A GaAs photoemission source with a high intensity of $10^{11} - 10^{12}$ electrons/pulse has been developed at SLAC for PNC experiments 19). Despite its many appealing characteristics, the usefulness of the GaAs source in certain low intensity applications is limited because the electron beam polarization is 0.3 - 0.4.

Because of its high polarization, PEGGY is scheduled to be used in additional high energy experiments at SLAC with a polarized proton and deuteron target. Recent improvements

have been made in the source which are expected to increase the intensity and the overall availability of PEGGY without degrading the high polarization. The uv interference filter has been removed and the 45° aluminized mirror has been replaced with a new multilayer dielectric mirror* which reflects selectively in the uv. The optical system is being further modified with the installation of a higher pressure Ar compressor for the vortex stabilized flashlamp. The atomic beam line has also been altered with the incorporation of active cooling for the first collimator to permit either the operation of the oven at higher temperatures and/or the use of a larger oven orifice, both of which would otherwise result in increased heating of the collimator and the consequent backscattering of skimmed atoms into the beam. (See Section 3.2.) Initial tests with the new 45° plane mirror and with the actively cooled collimator have shown that an electron beam intensity of $> 5 \times 10^{9}$ electrons/pulse for an oven temperature of $900^{\circ}C$ is readily achieved at the source without decreasing the polarization.

A more extensive development of PEGGY to increase its electron intensity by an order of magnitude and to provide rapid pulse to pulse polarization reversal without affecting the emittance of the electron beam has been considered 68).

---

*Developed by Acton Research Corporation, Acton, MA 01720. The reflectivity in the useful uv range of 170-230 nm is ~85%, while at 670 nm it is ~2%.

A two-step photoionization process through the 2P state using a tuned laser for the 2S-2P transition and the PEGGY flashlamp for the 2P-continuum transition could increase the intensity substantially. Polarization reversal might be obtained either by optical pumping of the Li atomic beam with the laser or by the inducing of radiofrequency transitions between hfs levels in the ground 2S state with only a small consequent reduction in polarization.

ACKNOWLEDGMENTS

Many people have contributed to the success of PEGGY during the long course of its development. We especially wish to thank H. Kobayakawa, D. Palmer and N. Sasao for their contributions during the early days of PEGGY's operation at SLAC. The electron optics studies by C. Tu also deserve special mention. We further wish to single out E. Garwin and the SLAC Physical Electronics Group for their important work in developing the vortex stabilized flashlamp.

The technical and engineering assistance provided by J. Brosious, R. Broughton, D. Constantino, S. Dhawan, A. Disco, S. Ladzinski, L. Trudell, and I. Winters of Yale University and M. Browne, R. Callen, R. Eisele, F. Johnson, R. Koontz, A. Lisin, T. McKinney, K. Porzuczek, R. Rowe, J. Sodja, and E. Taylor of SLAC and by P. Kliette of Universität Bielefeld was invaluable. Finally we wish to acknowledge the help and advice of J. Osantowski and the NASA optics group, of M. E. Mack of United Aircraft Research Laboratories (presently at Avco-Everett Research Laboratory), and of J. L. Emmett and J. B. Trenholme of Naval Research Laboratory (presently at Lawrence Livermore Laboratory), as well as of B. Flint and L. Stelmack of Acton Research Corporation.

LIST OF REFERENCES

1. M.J. Alguard et al., Phys. Rev. Lett. 37 (1976) 1258.
2. M.J. Alguard et al., Phys. Rev. Lett. 37 (1976) 1261.
3. M.J. Alguard et al., Phys. Rev. Lett. 41 (1978) 70.
4. J. Kuti and V.F. Weisskopf, Phys. Rev. D 4 (1971) 3418.
5. T.F. Walsh and P. Zerwas, DESY 72/36 (1972).
6. F.E. Close, Nucl. Phys. B80 (1974) 269.
7. A.J.G. Hey, Daresbury Lecture Note Series 13, DL/R33 (1974).
8. L.M. Sehgal, Phys. Rev. D 10 (1974) 1663.
9. R. Carlitz and J. Kaur, Phys. Rev. Lett. 38 (1977) 673, 1102.
10. R.J. Hughes, Phys. Rev. D 16 (1977) 622.
11. J. Schwinger, Nucl. Phys. B123 (1977) 223.
12. J.D. Bjorken, Phys. Rev. D 1 (1970) 1376.
13. J.D. Bjorken, Phys. Rev. Lett. 16 (1966) 408.
14. L. Gálfi, J. Kuti, and A. Patkós, Phys. Lett. 31B (1970) 465.
15. A. Bartl and W. Majerotto, Nucl. Phys. B62 (1973) 267.
16. H. Fraas, Nucl. Phys. B113 (1976) 532.
17. Ya. B. Bushnin et al., Yad. Fiz. 24 (1976) 536 [Sov. J. Nucl. Phys. 24 (1976) 279].
18. W.B. Atwood et al., Phys. Rev. D 18 (1978) 2233.
19. C.Y. Prescott et al., Phys. Lett. B77 (1978) 347.

20. Ya. B. Zel'dovich, Z. Eksp. Teor. Fiz. 36 (1959) 964 [Sov. Phys.-JETP 9 (1959) 682].

21. E. Derman, Phys. Rev. D 7 (1973) 2755.

22. R.N. Cahn and F.J. Gilman, Phys. Rev. D 17 (1978) 1313.

23. P.S. Cooper et al., Phys. Rev. Lett. 34 (1975) 1589.

24. M.R. Bergstrom et al., Bull Am. Phys. Soc. 23 (1978) 529.

25. V.W. Hughes, Proc. IInd Int. Conf. on Polarized Targets, Berkeley (1971), p. 191.

26. V.W. Hughes et al., Phys. Rev. A 5 (1972) 195.

27. J. Kessler, in Atomic Physics 3 (eds. S.J. Smith and G.K. Walters; Plenum Press, New York, 1973), p. 523.

28. J. Kessler, Polarized Electrons (Springer-Verlag, Berlin, 1976).

29. D.T. Pierce and F. Meier, Phys. Rev. B 13 (1976) 5484.

30. M.S. Lubell, in Atomic Physics 5 (eds. R. Marrus, M. Prior, and H. Shugart; Plenum Press, New York, 1977), p. 325.

31. G. Baum et al., Appl. Phys. 14 (1977) 149.

32. P.F. Wainwright et al., Rev. Sci. Instrum. 49 (1978) 571.

33. W. Raith, in Physics of One- and Two-Electron Atoms (eds. F. Bopp and H. Kleinpoppen; North-Holland, Amsterdam, 1969), p. 727.

34. The Stanford Two-Mile Accelerator, (ed. R.B. Neal; W.A. Benjamin, New York, 1968).

35. R.H. Miller, J. Berk, and T.O. McKinney, IEEE Trans. Nucl. Sci. NS-14 (1967) 98.

36. W.W. Ash, AIP Conf. Proc. No. 35, Subseries No. 12, High Energy Physics with Polarized Beams and Targets, Argonne (1976), p. 485.

37. E. Fues and H. Heilman, Phys. Z. 31 (1930) 465.

38. V.W. Hughes et al., Measurement of Asymmetry in Deep Inelastic Scattering of Polarized Electrons by Polarized Protons, SLAC Proposal No. E-80 (1971).

39. H. Deichsel and E. Reichert, Z. Phys. 185 (1965) 169.

40. H. Steidl, E. Reichert, and H. Deichsel, Phys. Lett. 17 (1965) 31.

41. K. Jost and J. Kessler, Phys. Rev. Lett. 15 (1965) 575.

42. J. Kessler and H. Lindner, Z. Phys. 183 (1965) 1.

43. K. Jost, Z. Phys. 195 (1966) 1.

44. W. Eitel, K. Jost, and J. Kessler, Phys. Rev. 159 (1967) 47.

45. H.D. Zeman, The Optimization of Low Energy Electron Scattering for Producing a Beam of Spin-Polarized Electrons, Ph.D. thesis (Stanford Univ., 1971), unpublished.

46. M.V. McCusker, L.L. Hatfield, and G.K. Walters, Phys. Rev. Lett. 22 (1969) 817.

47. M.S. Lubell and W. Raith, Phys. Rev. Lett. 23 (1969) 211.

48. G. Baum, M.S. Lubell, and W. Raith, Bull. Am. Phys. Soc. 16 (1971) 586.

49. U. Heinzmann, J. Kessler, and J. Lorenz, Z. Phys. 240 (1970) 42.

50. J. Kessler, Phys. Rev. Lett. 24 (1970) 87.

51. R.L. Long, Jr., W. Raith, and V.W. Hughes, Phys. Rev. Lett. 15 (1965) 1.

52. G. Baum and U. Koch, Nucl. Instrum. and Meth. 71 (1969) 189.

53. W. von Drachenfels et al., Nucl. Instrum. and Meth. 140 (1977) 47.

54. T.M. Müller, Eine technisch nutzbare Quelle zur Erzeugung polarisierter Elektronen, Ph.D. thesis (BONN IR-78-12, 1978), unpublished.

55. W. Brefeld et al., BONN-HE-78-16 (1978).

56. M.J. Alguard et al., Phys. Rev. Lett. 39 (1977) 334.

57. C.K. Sinclair et al., AIP Conf. Proc. No. 35, Subseries No. 12, High Energy Physics with Polarized Beams and Targets, Argonne (1976), p. 424.

58. E. Kisker et al., Phys. Rev. B 18 (1978) 2256.

59. R.L. Calvert, G.J. Russell, and D. Haneman, Phys. Rev. Lett. 39 (1977) 1226.

60. R. Feder, N. Müller, and D. Wolf, Z. Phys. B28 (1977) 265.

61. R.J. Celotta, U.S. National Bureau of Standards, Washington, D.C., private communication.

62. M. Kalisvaart et al., Phys. Rev. B 17 (1978) 1570.

63. M.J. Alguard et al., Proc. IXth Int. Conf. on High Energy Accelerators, Stanford (1974), p. 309.

64. J.S. Ladish, Production of Polarized Electrons, Ph.D. thesis (Yale Univ., 1974), unpublished.

65. G. Baum, M.S. Lubell, and W. Raith, Phys. Rev. A 5 (1972) 1073.

66. R.W. Ditchburn, Proc. R. Soc. Lond. 117 (1927) 486.

67. R.D. Hudson and V.L. Carter, Phys. Rev. 137 (1965) A1648.

68. M.J. Alguard et al., Phys. Rev. A 16 (1977) 209.

69. H. Frauenfelder and A. Rossi, in Methods of Experimental Physics 5, Part B (eds. L.C.L. Yuan and C.S. Wu; Academic Press, New York), p. 214.

70. N.F. Mott and H.S.W. Massey, The Theory of Atomic Collisions, 3rd ed. (Clarendon Press, Oxford, 1965).

71. W. Eckstein, IPP 7/2, Inst. f. Plasmaphys., München (1970).

72. G. Holzwarth and H.J. Meister, Nucl. Phys. 59 (1964) 56.

73. D.M. Schwartz, Phys. Rev. 162 (1967) 1306.

74. Nuclear Engineering Handbook (ed. H. Etherington; McGraw-Hill, New York, 1958), p. 13-83.

75. H. Lew, in Methods of Experimental Physics 4, Part A (eds. V.W. Hughes and H.L. Schultz; Academic Press, New York, 1967), p. 156ff.

76. Smithsonian Physical Tables, 9th ed. (ed. W.F. Forsythe, Smithsonian Institution, Washington, D.C., 1954), Table 697.

77. N.F. Ramsey, Molecular Beams (Oxford Univ. Press, London and New York, 1956), p. 28.

78. S. Dushman, Scientific Foundations of Vacuum Technology, 2nd ed. (John Wiley, New York, 1962), p. 80f.

79. P. Kusch and V.W. Hughes, Handbuch der Physik 37/1 (ed. S. Flügge; Springer-Verlag, Berlin, 1959), p. 28ff.

80. W. Schroen, Z. Phys. 176 (1963) 237.

81. J.B. Trenholme and J.L. Emmett, Ultra Violet Output from Pulsed Short Arcs, Naval Research Laboratory Memo No. 2427 (1972).

82. M.E. Mack, Appl. Opt. 13 (1974) 46.

83. E.L. Garwin, Stanford Linear Accelerator Center, private communication.

84. R.W. Bradford et al., in The Stanford Two-Mile Accelerator (ed. R.B. Neal; W.A. Benjamin, New York, 1968) p. 411.

85. W.B. Herrmannsfeldt, SLAC Report No. 166 (1973).

86. L. Mikaelyan, A. Borovoi, and E. Denisov, Nucl. Phys. 47 (1963) 328.

87. H. Boersch, R. Schliepe, and K.E. Schriefl, Nucl. Phys. A163 (1971) 625.

88. Tables of Asymmetry, Cross-section and Related Functions for Mott Scattering of Electrons by Screened Gold and Mercury Nucleii (eds. G. Holzwarth and H.J. Meister; Inst. f. Theo. Phys., Munchen, 1964).

89. B. Mühischlegel and H. Koppe, Z. Phys. 150 (1958) 474.

90. F. Gürsey, Phys. Rev. 107 (1957) 1734.

91. G. Knop and W. Paul, in Alpha-, Beta-, and Gamma-Ray Spectroscopy 1 (ed. K. Siegbahm; North-Holland, Amsterdam, 1965), pp. 1-25.

92. M.J. Alguard et al., IEEE Trans. Nucl. Sci. NS-24 (1977) 1603.

93. G.F. Hanne and J. Kessler, J. Phys. B 9 (1976) 791.

94. W.A. Bonner, M.A. Van Dort, and M.R. Yearian, Nature 258 (1975) 419.

95. L.A. Hodge, F.B. Dunning, and G.K. Walters, Rev. Sci. Instrum. (in press).

96. M. Erbudak and B. Reihl, Appl. Phys. Lett. 33 (1978) 584.

97. D.T. Pierce, U.S. National Bureau of Standards, Washington, D.C., private communication.

98. E. Reichert, Joh. Gutenberg Univ., Mainz, private communication.

99. M. Eminyan, École Polytechnique, Palaiseau, private communication.

100. E. Garwin et al., Nucl. Instrum. and Meth. 120 (1974) 483.

101. G.V. Marr and D.M. Creek, Proc. R. Soc. Lond. A 304 (1968) 233.

102. R.D. Hudson and V.L. Carter, J. Opt. Soc. Am. 57 (1967) 651.

103. D.E. Rothe, J. Quant. Spectrosc. Radiat. Transfer 11 (1971) 355.

104. J.H. Tait, in Atomic Collision Processes, Proc. of IIIrd Int. Conf. on The Physics of Electronic and Atomic Collisions (ed. M.R.C. McDowell; North-Holland, Amsterdam, 1964), p. 586.

105. A. Bhatia, A. Temkin and A. Silver, Phys. Rev. A 12 (1975) 2044.

106. B. Ya'akobi, Proc. Phys. Soc. Lond. 92 (1967) 100.

107. T.C. Caves, A. Dalgarno, J. Quant. Spectrosc. Radiat. Transfer 12 (1972) 1539.

108. D.W. Norcross, Joint Institute for Laboratory Astrophysics, Boulder, private communication.

Appendix

ELECTRON BEAM DEPOLARIZATION IN THE STANFORD TWO-MILE ELECTRON ACCELERATOR

A.1 INTRODUCTION

The 70 keV electron beam emerging from the polarized electron gun is highly longitudinally polarized. We will consider here the possible depolarization of this beam as it is accelerated to high energies in the SLAC accelerator. For our application we define the depolarization as the decrease in the component of the electron polarization or spin along the beam direction. Our principal result is an upper bound on the depolarization calculated in terms of known beam parameters as far as is possible.

A.2 POLARIZATION EQUATIONS OF MOTION

For an electron at rest we define the polarization or spin vector $\vec{S}$ to be the expectation value of the spin operator. The equation of spin motion 1,2) is:

$$\frac{d\vec{S}}{dt} = \mu_o g \vec{S} \times \vec{B} \quad . \qquad \text{(rest frame)} \qquad (1)$$

in which μ_o = electron Bohr magneton, g = electron gyromagnetic ratio = 2(1+a) where a = electron anomalous g-value, and $\vec{B}$ = magnetic field in electron rest frame.

In the laboratory frame of reference where the electron velocity is $\vec{v}$, the orbital and spin equations of motion are:

$$\frac{d\vec{p}}{dt} = e\left(\vec{E} + \frac{\vec{v} \times \vec{B}}{c}\right) \qquad (2)$$

$$\frac{d\vec{S}}{dt} = \vec{S} \times \frac{e}{mc\gamma}\left[(1+\gamma a)\vec{B} - \frac{a(\gamma-1)}{v^2}\vec{v}\cdot\vec{v}\,\vec{B} - \frac{\gamma}{c}\left(\frac{1}{1+\gamma}+a\right)\vec{v}\times\vec{E}\right] \qquad (3)$$

(laboratory frame)

in which $\vec{S}$ is the spin vector in the electron rest frame, and all other quantities refer to the laboratory frame. We note from Eq. (3) that an electric field along the direction of motion will not change the polarization vector and also that under the influence of general external electric and magnetic fields the polarization vector can change in direction but not in magnitude. However, if the electron beam has a finite extent, different particles will have different orbits in different fields and hence the polarization vector averaged over the whole beam can change in both magnitude and direction.

We shall be interested in only the longitudinal polarization which can be described by the angle between the polarization and momentum vectors. Define two unit vectors $\hat{\ell}$ and $\hat{n}$ such that $\hat{\ell}$ is in the direction of the momentum and $\hat{n}$ is normal to $\hat{\ell}$ and in the plane of $\hat{\ell}$ and the polarization $\vec{S}$. Then we have

$$\vec{S} = S(\hat{\ell}\cos\theta + \hat{n}\sin\theta) \qquad (4)$$

where θ is the angle between $\vec{S}$ and $\hat{\ell}$. If this expression is substituted into Eq. (3), the following equation for θ is obtained:

$$\frac{d\theta}{dt} = \frac{ea}{mc\beta}(\hat{n}\cdot\vec{E} + \beta\hat{\ell}\cdot\vec{B}\times\hat{n}) - \frac{eg}{2mc\beta\gamma^2}\hat{n}\cdot\vec{E} \quad . \qquad (5)$$

The change Δ in the angle during the particle orbit is

$$\Delta = \int dt\,(d\theta/dt) = \frac{1}{mc}\int dt\,\hat{n}\cdot\left(\frac{a}{\beta}\frac{d\vec{p}}{dt} + \frac{eg}{2\gamma^2\beta}\vec{E}\right) = \Delta_a + \Delta_g \quad . \qquad (6)$$

The associated depolarization is $D = 1-\cos\Delta$.

A.3 DEPOLARIZATION CALCULATION

Calculation of the first term in Eq. (6), which we call Δ_a since it is proportional to the anomalous g-factor a, requires no knowledge of the electromagnetic fields seen

by the particle. It may be bounded as follows:

$$\left|\Delta_a\right| \leq \frac{a}{mc\beta_{min}} \left(\left|\Delta p_r\right| + \left| \int \frac{p_r}{p} \, dp_z \right| \right)$$

$$\leq \frac{a}{mc\beta_{min}} \left(\left|\Delta p_r\right| + p_r^{max} \ln \frac{\beta\gamma}{\beta_o\gamma_o} \right) \tag{7}$$

in which z is along the axial direction of the accelerator and r is in the radial direction. For SLAC 3) with an injection energy of 70 keV and a final energy of 20 GeV, $\beta_{min} = \beta_o = 0.5$, $\gamma_o = 1.16$ and $\gamma = 4 \times 10^4$. The maximum radial momentum for particles in the beam is about $p_r^{max} = 0.5$ MeV/c or 0.3 mc and the maximum change in the radial momentum Δp_r^{max} is twice this value. Hence we obtain

$$\left|\Delta_a\right| \leq 9 \times 10^{-3} \tag{8}$$

which corresponds to $D = 4 \times 10^{-5}$, a negligibly small depolarization.

The second term in Eq. (6), which we will call Δ_g, depends on the component of the electric field normal to the momentum. We may bound this term as follows

$$\left|\Delta_g\right| = \frac{g}{2} \int \frac{d(\beta\gamma)}{\gamma^2\beta} \frac{\hat{n} \cdot \vec{E}}{\hat{\ell} \cdot \vec{E}} \leq \frac{g}{2} I(\gamma_o, \gamma) \tan\alpha \tag{9}$$

where α is the maximum angle between the momentum and the electric field vectors and I is the integral

$$I(\gamma_1,\gamma_2) = \int_{\gamma=\gamma_1}^{\gamma=\gamma_2} \frac{d(\beta\gamma)}{\gamma^2\beta} = \frac{1}{2} \ln\left(\frac{\gamma_2-1}{\gamma_2+1}\,\frac{\gamma_1+1}{\gamma_1-1}\right) \quad . \quad (10)$$

If α_E and α_p are the maximum angles that the electric field and momentum vectors form with respect to the optical axis than we have approximately

$$\alpha = \left(\alpha_E^2 + \alpha_p^2\right)^{1/2} \quad . \quad (11)$$

This follows from the linearity of the motion and the assumption that the radial electric field varies linearly with the radial coordinate r. The approximate expression for α_E is given by

$$\sin \alpha_E = \frac{E_r}{E} = \frac{r\omega}{2u} \sin \phi \quad (12)$$

where u is the phase velocity in the microwave cavities, ω is the angular frequency of the accelerating field and ϕ is the particle phase (zero phase corresponds to maximum acceleration). For the SLAC accelerator we have $\omega/c = 0.6\ \text{cm}^{-1}$.

The acceleration process can be considered in two parts. The first involves the low energy unbunched motion occurring in the prebuncher, buncher, and approximately the first

10 cm of the accelerator section of the injection. The second part involves the high energy bunched motion in the remainder of the injector and in the main accelerator. We consider the high energy part first. Here γ increases from about 3.5 to its final ultrarelativistic value. The relevant energy dependent factor is $I(3.5,\infty) = 0.294$. For the maximum transverse momentum we may take $p_r \leq 0.3$ mc (0.15 MeV/c). The minimum momentum in this region is $p = mc\beta\gamma = 3.35$ mc. Therefore $\alpha_p = p_r/p = 0.090$. To obtain α_E we use the facts that the phase velocity is the speed of light, the beam radius is less than 0.5 cm, the phase ϕ is less than 5^o, and $\omega/c = 0.6$ cm^{-1}. This gives $\alpha_E = 0.013$, and thus from Eq. (11) $\alpha = 0.091$. Hence from Eq. (9) the contribution to $|\Delta_g|$ from the high energy portion is only 0.027, which corresponds to a depolarization of $D = 3.6 \times 10^{-4}$.

In the low energy region the energy dependent factor is $I(1.16, 3.5) = 1.00$. The transverse momentum in this region is limited to $p_r \leq 0.05$ mc (0.026 MeV/c) so that $\alpha_p = 0.086$. Because the beam is unbunched we cannot set a small bound on $\sin\theta$ and we set it equal to unity. Using the buncher value of the phase velocity $u = 0.75$ c and a beam radius of 0.5 cm we obtain $\alpha_E = 0.20$. In the microwave coupler cavities Eq. (12) is not exactly true because there is a slight azimuthal asymmetry but this does not significantly affect our estimate of α_E. We have then $\alpha = 0.218$, and hence $|\Delta_g| = 0.218$.

Adding the low and high energy contributions together gives

$$|\Delta| = |\Delta_g| \leq 0.245 \qquad (13)$$

which corresponds to a depolarization D of 3×10^{-2}.

Calculations of the depolarization have also been made in terms of the estimated electromagnetic fields seen by the electron 4). This approach leads to smaller values for the depolarization because it takes into account more of the correlations between the orbit motion and the fields. The approximations made, however, are such that the bound obtained by this calculation is not reliable.

A.4 DISCUSSION

We have estimated for the SLAC accelerator an upper bound to the change Δ in the angle between the polarization and momentum vectors based on known beam parameters and including extreme electron trajectories. Averaged over the whole beam the corresponding average depolarization in acceleration from 70 keV to 20 GeV will be less than 3×10^{-2}.

The angle Δ has been written as the sum of two parts, Δ_a and Δ_g. The calculation of the purely anomalous part Δ_a does not require knowledge of the fields seen by the particle but only of the maximum transverse momentum in the beam and of the initial and final energies. This term is small

because a is small and the electrons are injected at a relativistic velocity of $\beta = 0.5$. The term Δ_g is proportional to g and the component of the electric field normal to the momentum. This term corresponds to the nonrelativistic effect in which the electric field changes the direction of the momentum but not of the spin. (The gyromagnetic ratio g enters only because part of this effect is contained in Δ_a. See Eq. (5).) Only the low energy region in which the bunching process takes place is important for this term. Because of the energy dependence of this term the bound obtained on the depolarization is small even though the beam transverse emittance grows downstream of the injector.

Acknowledgements

This work has been completed in part due to contributions by R. Helm. We are also indebted to unpublished works on this problem by W.K.H. Panofsky and E. M. McMillan.

References

1. V. Bargmann, L. Michel, and V.L. Telegdi, Phys. Rev. Lett. 2 (1959) 435.
2. R. Hagedorn, Relativistic Kinematics (W. A. Benjamin, New York, 1963), chapter 9.
3. The Stanford Two-Mile Accelerator (ed. R.B. Neal; W.A. Benjamin, New York, 1968).
4. R.H. Helm and W.P. Lysenko, SLAC-TN-72-1 (1972).

TABLE I. Characteristics of Polarized Electron Sources

METHOD		GROUP	REFERENCE	MODE		PULSE LENGTH (μsec)	INTENSITY (10^9 e/pulse)	REP RATE (pps)	AVERAGE CURRENT (nA)	DEGREE OF POLARIZATION	METHOD OF POLARIZATION REVERSAL				ELECTRON ENERGY (eV)	ENERGY SPREAD (eV)	MAGNETIC FIELD (G)	EMITTANCE AT STATED ENERGY (mrad-cm)	BRIGHTNESS		
				PULSED	dc						ANGLE	ENERGY	MAGNETIC	OPTICAL					MEDIUM	HIGH	VERY HIGH
Electron Scattering from Unpolarized Hg Beam		Münster	93		●				0.01-0.1	0.22	●	●			5	0.6-1.0	~0	30		●	
		Stanford	94		●				10-35	0.1-0.23	●	●			50-180	—	~0	—		●	
Photoionization	Fano Effect Rb	Bonn	53,54	●		0.012	2.2	50	18	0.65				●	$120x10^3$	<500	120	1.0	●		
	Fano Effect Cs	Yale	32		●				25	0.63				●	1000	3	0.05	<20		●	
	Polarized Li Beam "PEGGY"	Yale-SLAC-Bielefeld		●		1.6	2.6	180	72	0.85			●		$70x10^3$	1500	200	<10	●		
Optically Pumped He Discharge		Rice	95		●				$2x10^3$ 10^4	0.4 0.3				●	400	<0.15	~0	2			●
Field Emission EuS		Bielefeld	31,58		●				10	0.85			●		3	0.1	~50	10^{-3}			●
Photoemission	GaAs[a]	ETH Zurich	96		●				10^4	0.35				●	30	0.2	~0	2			●
		NBS Gaithersburg	97		●				10^4	0.43				●	1	0.18	~0	20			●
		SLAC	19	●		1.6	1000	120	$2x10^4$	0.37				●	$65x10^3$	0.2	~0	<7			●
		Mainz	98		●				$>10^3$	0.4				●	—	0.2	~0	—			●
		PMC Palaiseau	99		●				$5x10^3$	—				●	7	0.2	~0	—			●
	EuO	ETH Zurich-SLAC	100	●		1.2	3	6.7	3.2	0.6			●		~2	~2	$21x10^3$	$1.5x10^4$	●		

(a) Additional GaAs sources are currently under development at Bielefeld-West Germany, Chalk River-Canada, Edinburgh-Scotland, FOM Amsterdam-Netherlands, and Yale-USA.

TABLE II. Oven, Collimator, and Sextupole Parameters

A.	Oven Parameters		
	Oven capacity at 925°C	750 g	
	Ratio of internal height to diameter	1	
	Wall thickness	1 cm	
	Length of Thermocoax heating cable in contact with oven	35 m	
	Power required at 875°C	600 W	
B.	Beam Collimating Parameters		
	Oven orifice diameter	1.7 mm	
	Oven orifice channel length	1.2 mm	
	Separation of oven orifice and collimator I	2.54 cm	
	Collimator I aperture diameter	2.26 mm	
	Separation of oven orifice and collimator II	8.1 cm	
	Collimator II aperture diameter	3.8 mm	
C.	Sextupole Magnet Parameters	Small Bore	Large Bore
	Gap between pole tips	3.2 mm	6.4 mm
	Length each section	7.6 cm	15.2 cm
	Number of sections	4	2
	Space between sections	1.3 cm	1.1 cm
	Magnetic field strength at pole tips	8600 G	8300 G
	Effective transmission angle to ionization region:		
	Ω^+, for m_J = + 1/2 atoms	2.9×10^{-4} sr	5.2×10^{-4} sr
	Ω^-, for m_J = - 1/2 atoms	6.2×10^{-7} sr	6.8×10^{-6} sr
	State selection parameter, s, for an ionization region of radius 0.3 cm	0.996	0.97
D.	Other Parameters		
	Distance from oven orifice to entrance of sextupole magnet	11 cm	
	Distance from sextupole magnet exit to center of ionization region	28 cm	
	Polarization of atomic beam, $P_{e,atom}$, in ionization region	0.95±0.04	0.92±0.04
	Distance from ionization region to atomic beam detector	36 cm	

TABLE III. Operating Characteristics

Atomic Beam	
Oven temperature	$875^{o}C$
Flux at photoionization region	7.0×10^{15} atoms s^{-1}
FWHM at ionization region	0.3 cm
Most probable beam velocity in ionization region	2×10^{5} cm s^{-1}
Number of atoms in photo-ionization region	10^{11}
Fraction of atoms photoionized	0.02
Lifetime of Li oven load[a]	175 h
Time to reload Li	43 h
Vortex Stabilized Ar Flashlamp	
Pulse length	1.6 μs
Repetition rate[b]	180 pps
Pulse to pulse intensity variation	< 5%
Typical lifetime	2×10^{7} pulses
Electron Beam	
Intensity[c] (electrons/pulse)	
at 70 keV	$(2.0 \pm 0.3) \times 10^{9}$ 2.6 ± 10^{9} maximum
At GeV energies	$(0.74 \pm 0.14) \times 10^{9}$ 1.1 ± 10^{9} maximum
Polarization at GeV energies	0.85 ± 0.07
Polarization reversal time	$\leq$ 1 s
Intensity difference upon reversal[d]	< 5%
Overall availability	75%

[a] Lifetime based on an oven load of 750 g Li.

[b] Modulator and flashlamp were usually operated at a repetition rate of 180 pps with 120 pps injected into the linac and 60 pps used for polarization measurement at low energy.

[c] The values of intensity are averaged over the latest 1000 h of PEGGY operation. The maximum values are averaged over shorter periods of 2-3 h.

[d] The intensity difference can be reduced to <2% by fine tuning the electron optics.

LIST OF FIGURES

peller and cathode are representative electron trajectories.

5. Lithium photoionization cross sections for the 2S ground state and the 2P excited state. Solid curves are experimental results and dashed curves are theoretical calculations with bands representing the spread in the measured and the calculated results. The experimental results are taken from Refs. 101) and 102) for the 2S ground state and from an empirical formula given in Ref. 103) for the 2P state. The theoretical calculations are taken from Refs. 104) and 105) for the 2S state, and from Refs. 106), 107), and 108) for the 2P state.

6. Schematic representation of the atomic excitation scheme (nuclear spin decoupled). The ground state atoms are assumed to be in the $m_J = +1/2$ state. Unpolarized 2S-2P resonant light incident parallel to the magnetic field induces the transitions indicated by the upward pointing arrows. The spontaneous decay transitions are indicated by the downward pointing arrows. The circled numbers denote the relative strengths of the transition. The electronic polarization of each state is given in the boxes.

7. Optical efficiency of the major components of the optics system: (a) ellipsoidal mirror; (b) uv filter; (c) vacuum window; (d) 45^{o} plane mirror. The dashed lines represent regions of less certainty.

8. The Møller asymmetry and laboratory cross section plotted versus scattering angle for the representative incident energy of 9.712 GeV, one of the energies at which Møller polarization measurements were made 23).

9. Scale drawing of PEGGY showing a top view and an elevation. The parallel offset of the PEGGY beam line from the injector beam line can be seen in the top view. Abbreviations which have been used are as follows: BKO, beam knock out for changing pulse duration and separation; FV, fast valve; IP, ion pump; L, magnetic lens; S, magnetic steering; SV, slow valve; T, toroid beam current monitor; and ZnS, zinc sulfide screen for visual monitoring of the beam.

10. Cross section of the oven and ionization vacuum chambers and of the optics chamber showing the atomic beam forming and optics components (the polarized electron beam exits to the right): (a) typical feed-through for oven heating current; (b) Thermocoax heating cable; (c) Freon cooling system; (d) copper box; (e) pivot; (f) horizontal positioning plate; (g) vertical adjustment; (h) funnel; (i) Li recovery bottle; (j) collimator I; (k) chopper wheel; (l) lamp; (m) photodiode, (n) motor and ferrofluidic feed-through; (o) collimator II; (p) sextupole magnet; (q) axis of butterfly value; (r) atomic beam; (s) vortex stabilized Ar flashlamp; (t) ellipsoidal mirror; (u) tilt; (v) horizontal posi-

tioning plates; (w) photodiode; (x) uv filter; (y) Suprasil window; (z) 45^{o} plane mirror; (aa) ground shield; (bb) repeller; (cc) cathode; (dd) anode; (ee) retro-reflector; (ff) ionization region; (gg) cylindrical coil; and (hh) retractable atomic beam detector.

11. Cross section of the larger lithium (750 g capacity) oven and the first collimator. The wire mesh "wick" and the spherical surface of the collimator assist the condensed Li to flow away from the aperture and into the Li recovery bottle.

12. Atomic beam collimating system. The diameter of the beam defining orifices are indicated. The heated elements are shaded by diagonal slashes.

13. Atomic beam intensity in atoms s^{-1} at the surface-ionization detector as a function of oven temperature T_0 for which the vapor pressure of lithium is p_0. The data are indicated by the closed circles. The uncertainty in the detector efficiency is shown for the datum at our typical operating temperature. The temperature scale for the data has an uncertainty of $\pm 15^{o}C$ associated with it. The solid curve is the variation for effusive flow conditions predicted by Eq. (8) and the calculated value of 2.9×10^{-4} sr for the effective solid angle for transmission of Li atoms through the large bore sextupole magnet to the detector region.

14. Cross section of the 3.2 mm bore sextupole permanent magnet.

15. Cross section of the 6.4 mm bore sextupole permanent magnet.

16. Atomic beam profile at (a) the surface-ionization detector located 36 cm downstream from the center of the ionization region and (b) the center of the ionization region. The curves are obtained from computer calculations for an oven temperature of 875°C, a Li vapor pressure of 8 Torr, a detector wire diameter of 0.13 mm and a transmission through the mechanical chopper of 0.06. No correction is made for the length of the hot wire. Surface-ionization detector measurements are shown as closed circles in (a). The measured intensity has an uncertainty of ±20% while the full width half maximum (FWHM) is correct within a few percent. The deviation from the predicted profile in the wings is probably due to collimation effects which were not taken into account in the computer calculations.

17. Cross section of the sealed lamp.

18. Cross section of the vortex stabilized argon flashlamp, shown together with the ellipsoidal mirror and part of the ionization chamber.

19. Sketch of the vortex flashlamp in operation.

20. Spectrum of the sealed lamp for a peak lamp current of 3.4 kA. The lines connecting data points are to guide

the eye. In the longer wavelength region where there are no connecting lines the absolute calibration is not well known.

21. Spectrum of the vortex flashlamp for a peak lamp current of 7.0 kA. The lines connecting data points are to guide the eye. In the longer wavelength region where there are no connecting lines the absolute calibration is not well known.

22. Block diagram of the modulator circuit for the vortex stabilized flashlamp. Abbreviations which have been used are as follows: P.S., power supply; D.C., direct current; L, inductance; and C, capacitance.

23. Vortex flashlamp current pulse and corresponding light pulse. The structure in the lamp current pulse is a result of ringing in the modulator circuit and does not appear in either the light or the photoelectron pulse.

24. Diagram showing the Mott scattering apparatus. The direction of the incident beam is perpendicular to the plane of the figure. Collimators are denoted by a "c". Note that the distance between the two scattering foils is 10 cm and the semiconductor detector surfaces are located 5.2 cm away from the center of the analyzing gold foil.

25. Mott scattering pulse height spectrum for 70 keV electrons as recorded by a 256 channel pulse height analyzer. Each point represents the sum of two adjacent

channels. The foil thicknesses for wheels $\mathscr{A}$ and $\mathscr{B}$ were 79 and 24 μg cm^{-2} respectively.

26. Experimental values of the Mott scattering asymmetry, $A_M(t)$, for the foil thicknesses, t, available at the target wheel $\mathscr{B}$. The error bars represent the statistical uncertainty (one standard deviation). The extrapolation constant, α, is determined by a straight line fit to be 0.0044 cm^2 μg^{-1}.

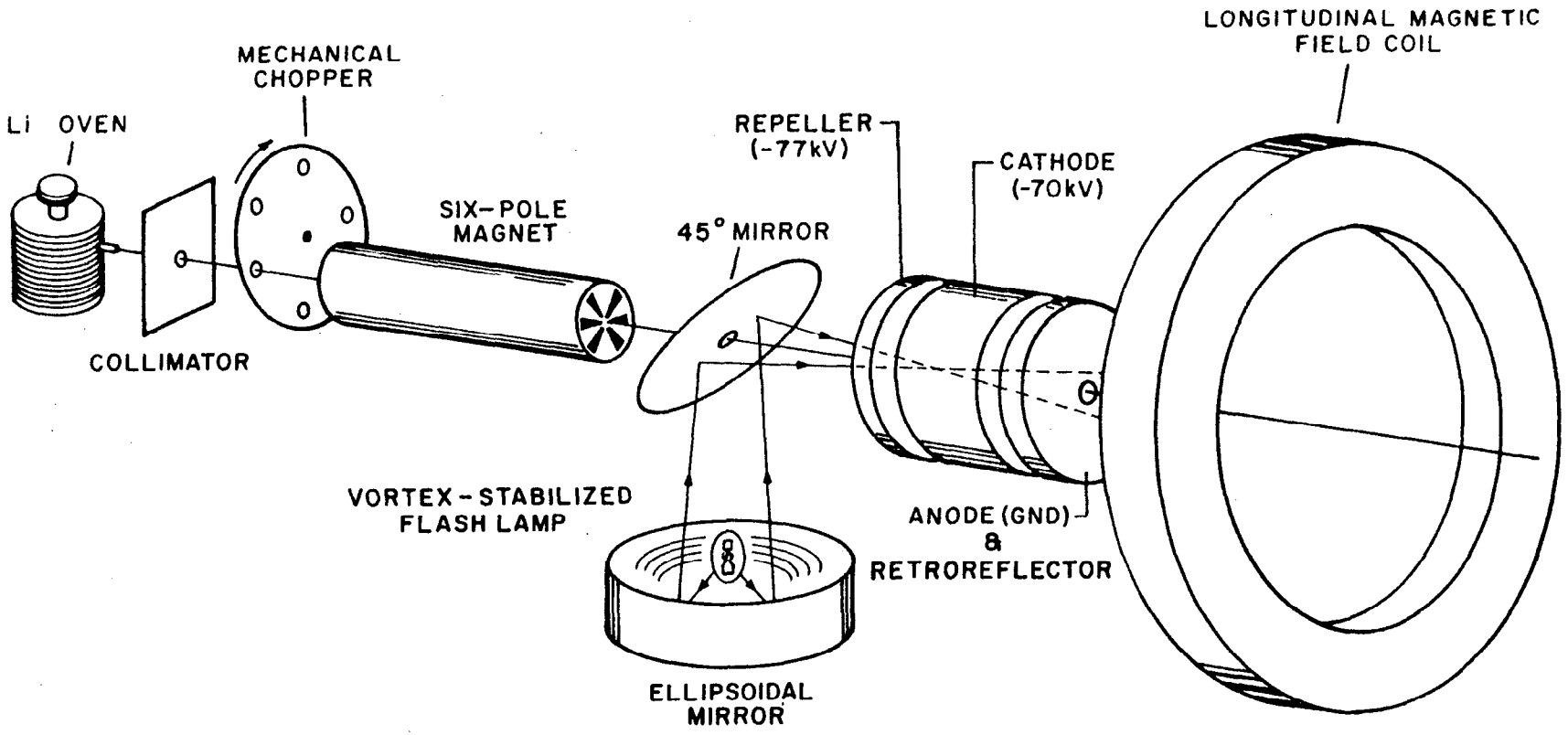
LONGITUDINAL MAGNETIC
FIELD COIL
MECHANICAL
CHOPPER
Li OVEN
REPELLER
(-77kV)
CATHODE
(-70kV)
SIX-POLE
MAGNET
45° MIRROR
COLLIMATOR
VORTEX-STABILIZED
FLASH LAMP
ANODE (GND)
&
RETROREFLECTOR
ELLIPSOIDAL
MIRROR

Fig. 1

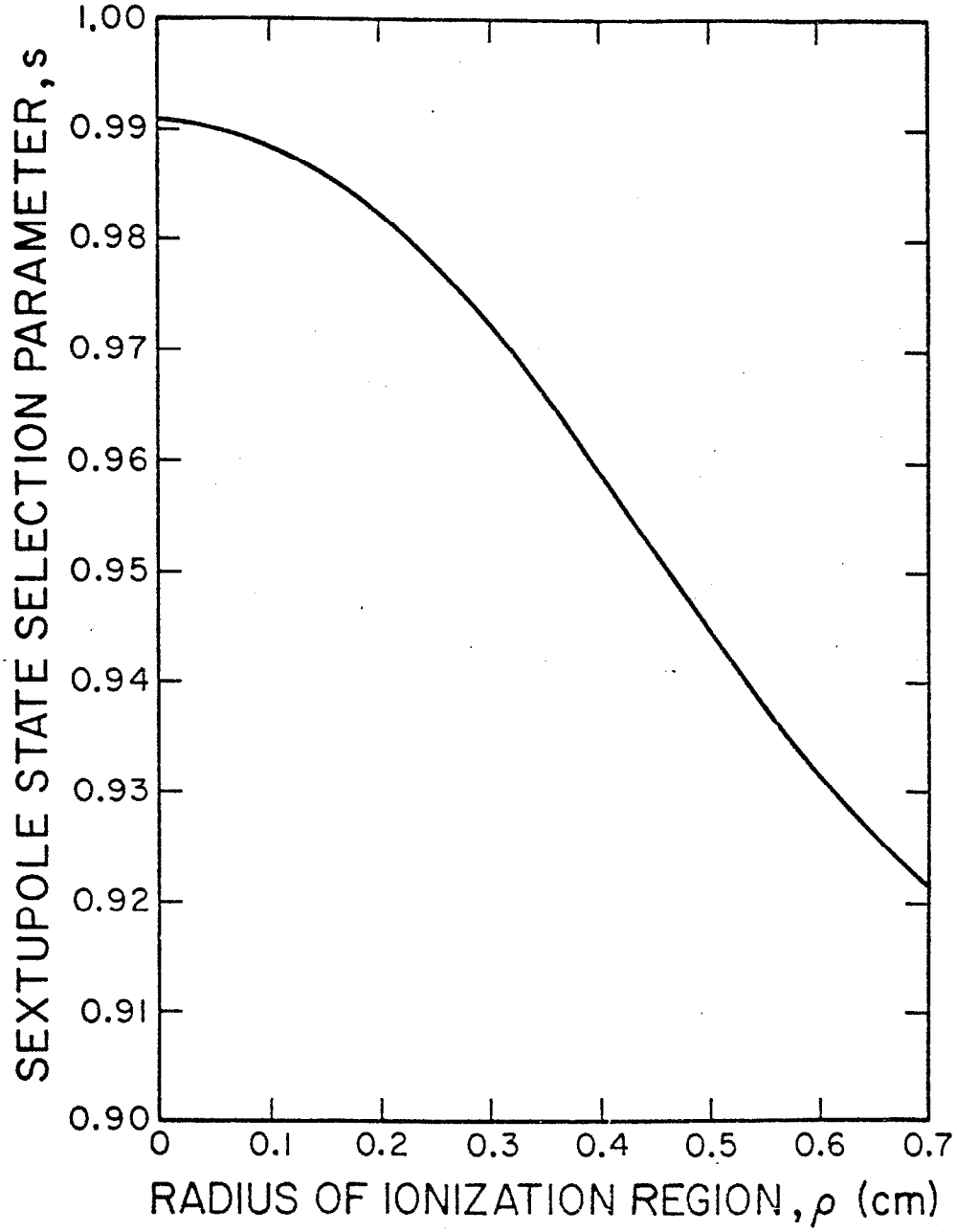
1.00
0.99
0.98
0.97
0.96
0.95
0.94
0.93
0.92
0.91
0.90
SEXTUPOLE STATE SELECTION PARAMETER, s
0
0.1
0.2
0.3
0.4
0.5
0.6
0.7
RADIUS OF IONIZATION REGION, ρ (cm)

Fig. 2

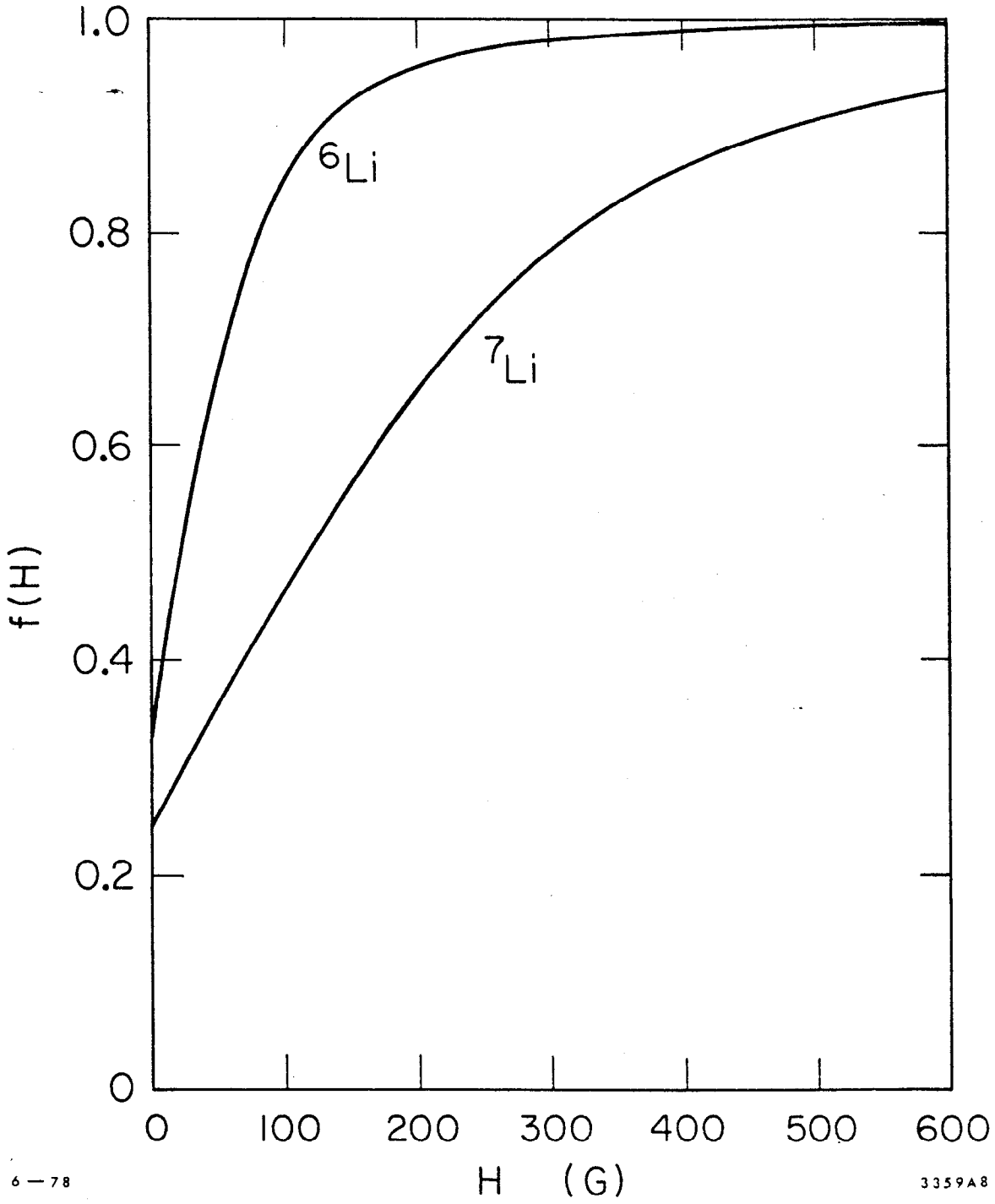

Fig. 3

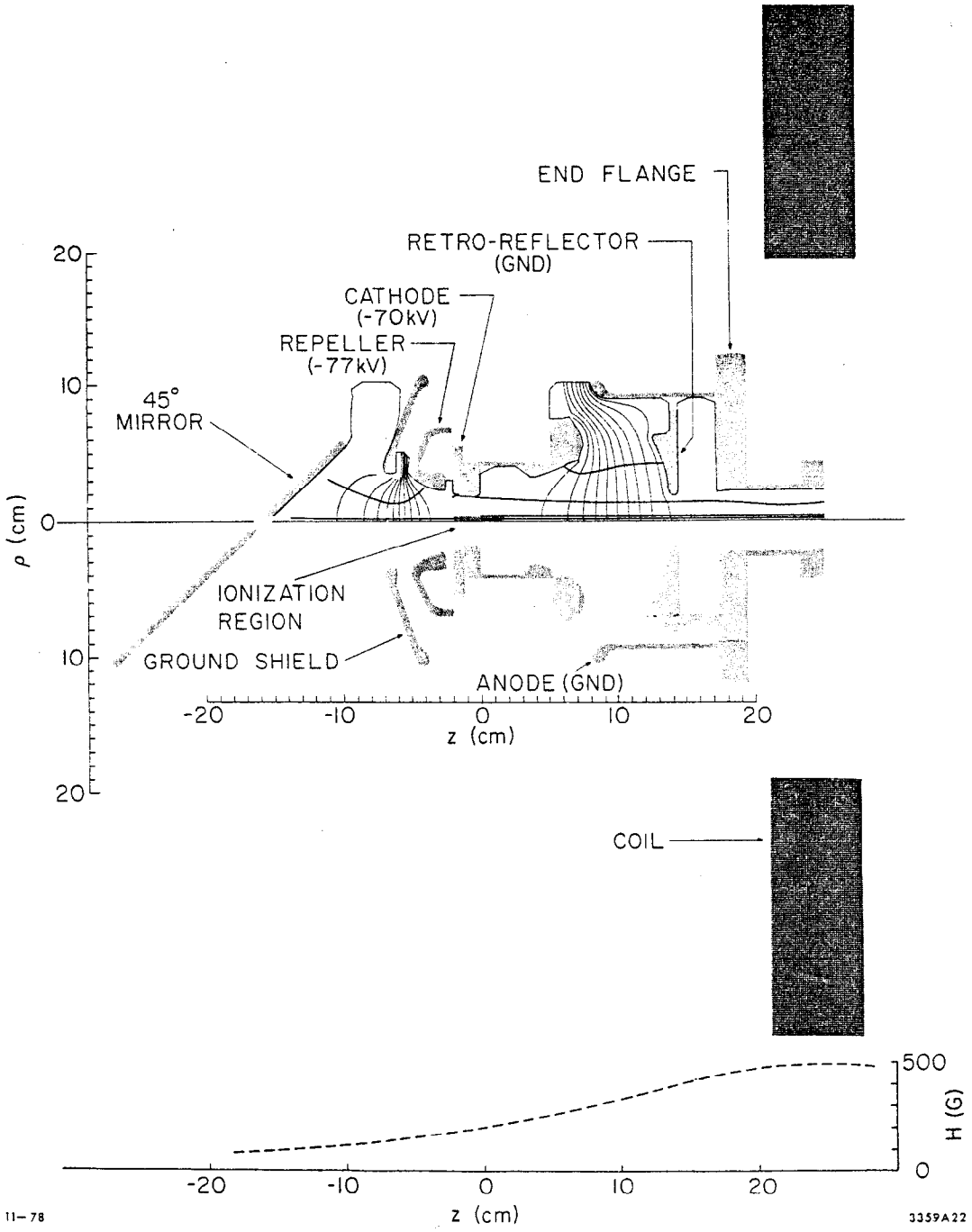
END FLANGE
RETRO-REFLECTOR
(GND)
CATHODE
(-70kV)
REPELLER
(-77kV)
45°
MIRROR
IONIZATION
REGION
GROUND SHIELD
ANODE (GND)
ρ (cm)
z (cm)
COIL
H (G)
500
0
11-78
3359A22

Fig. 4

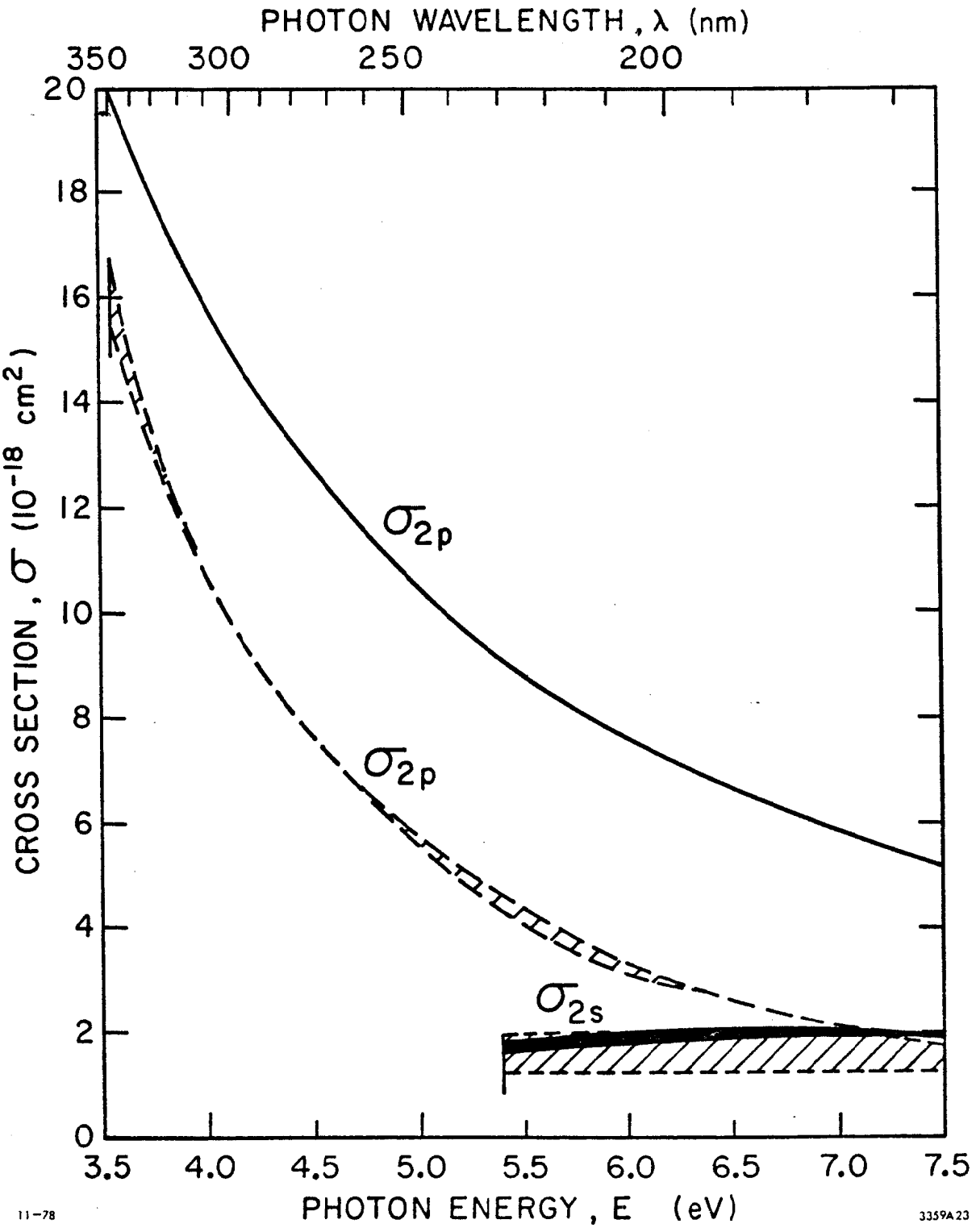
PHOTON WAVELENGTH , λ (nm)
350
300
250
200
20
18
16
14
12
10
8
6
4
2
0
CROSS SECTION , σ (10⁻¹⁸ cm²)
σ2p
σ2p
σ2s
3.5
4.0
4.5
5.0
5.5
6.0
6.5
7.0
7.5
PHOTON ENERGY , E (eV)
11-78
3359A23

Fig. 5

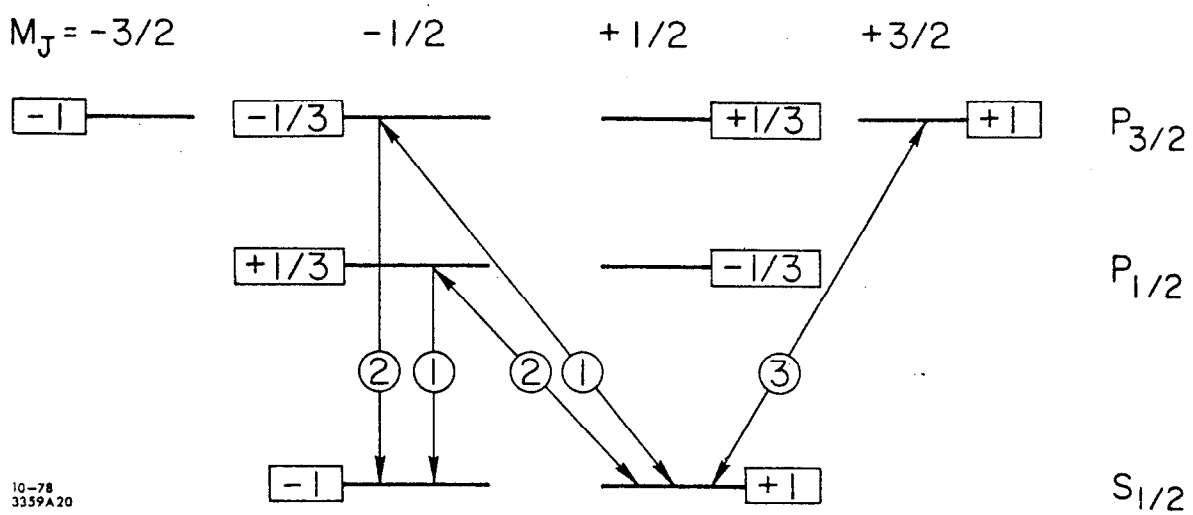

Fig. 6

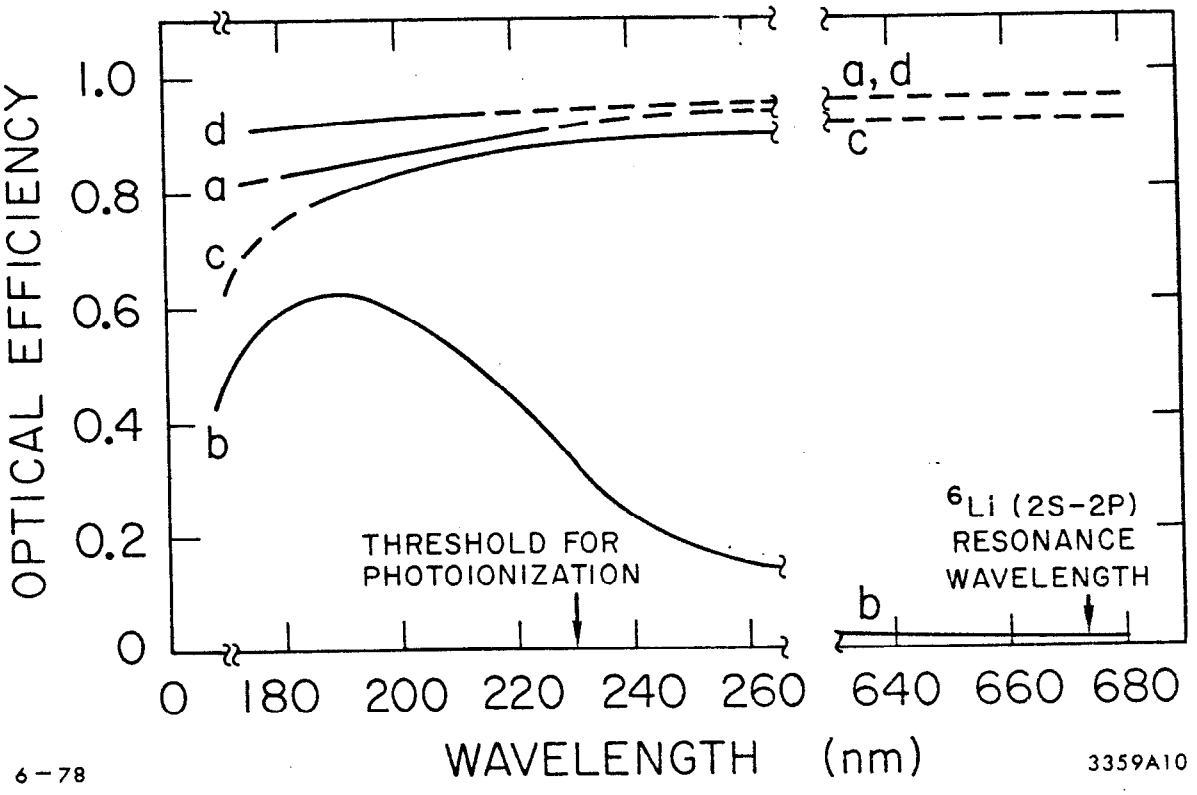
OPTICAL EFFICIENCY
1.0
0.8
0.6
0.4
0.2
0
d
a
c
b
a, d
c
b
THRESHOLD FOR
PHOTOIONIZATION
^{6}Li (2S-2P)
RESONANCE
WAVELENGTH
0
180
200
220
240
260
640
660
680
WAVELENGTH (nm)
6-78
3359A10

Fig. 7

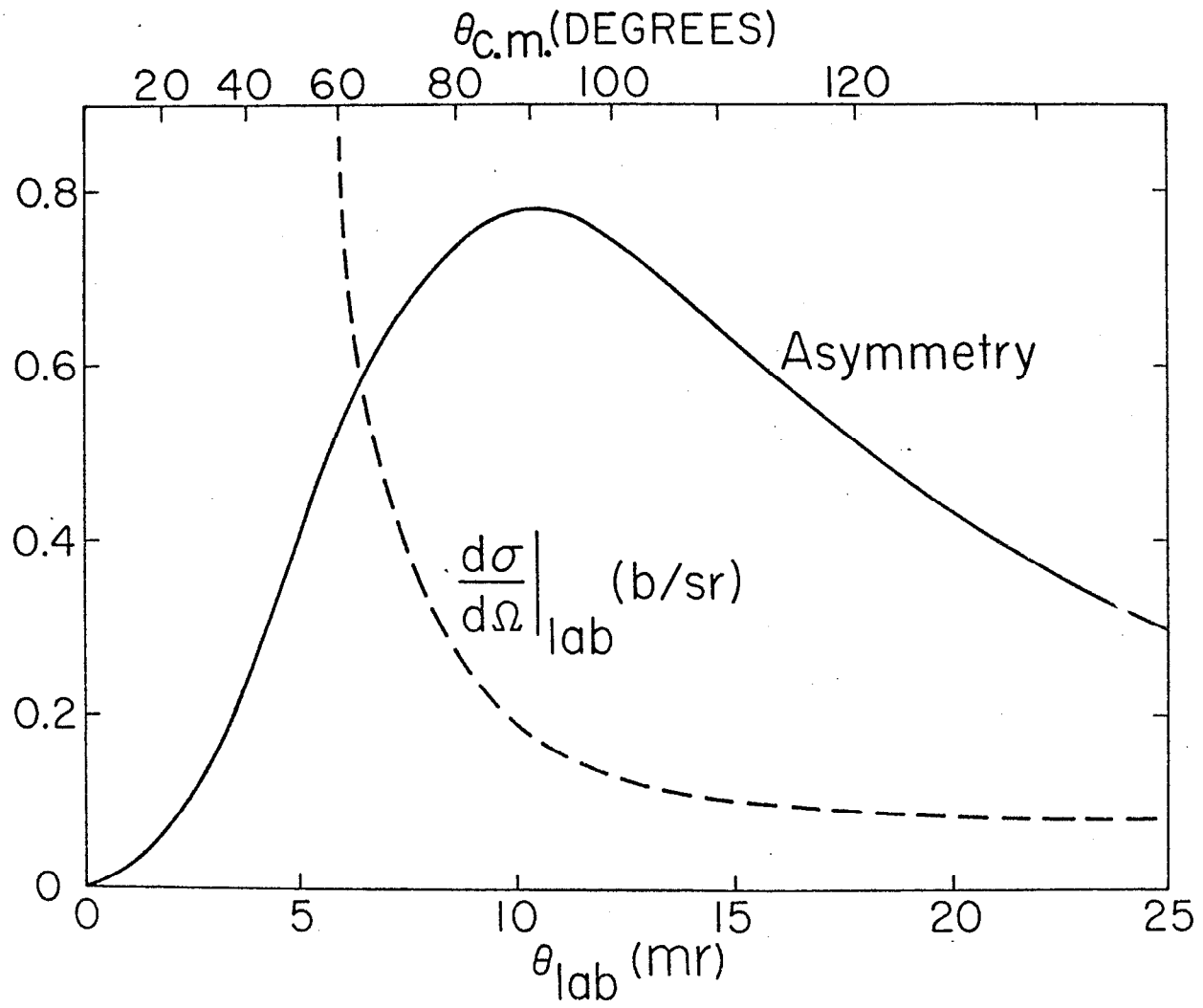
θc.m.(DEGREES)
20 40 60 80 100 120
0.8
0.6
0.4
0.2
0
Asymmetry
dσ/dΩ|lab (b/sr)
0 5 10 15 20 25
θlab (mr)

Fig. 8

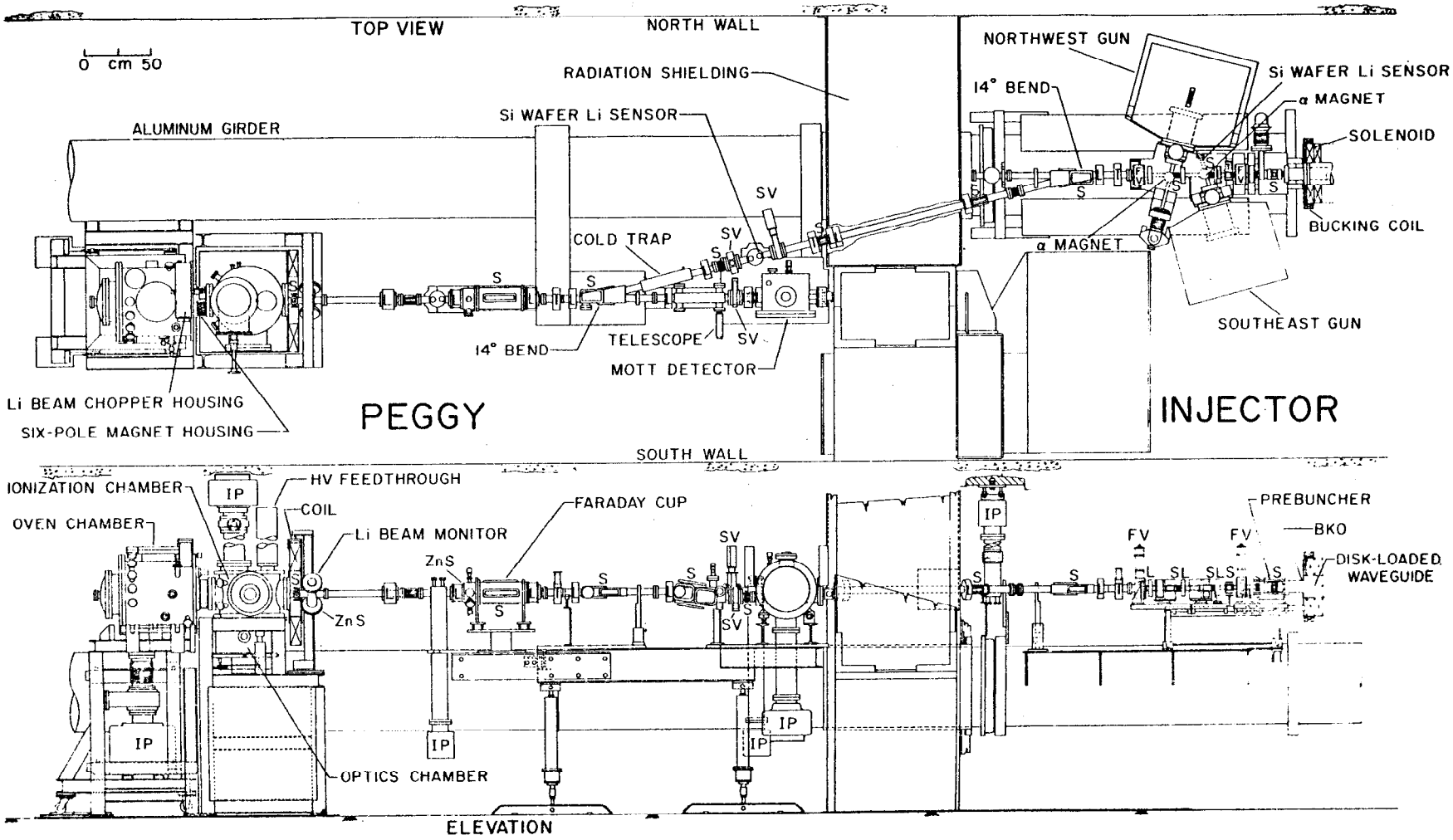
TOP VIEW
0 cm 50
NORTH WALL
RADIATION SHIELDING
NORTHWEST GUN
Si WAFER Li SENSOR
14° BEND
α MAGNET
SOLENOID
ALUMINUM GIRDER
Si WAFER Li SENSOR
SV
COLD TRAP
BUCKING COIL
α MAGNET
SOUTHEAST GUN
14° BEND
TELESCOPE
MOTT DETECTOR
Li BEAM CHOPPER HOUSING
SIX-POLE MAGNET HOUSING
PEGGY
INJECTOR
SOUTH WALL
IONIZATION CHAMBER
HV FEEDTHROUGH
COIL
OVEN CHAMBER
Li BEAM MONITOR
FARADAY CUP
PREBUNCHER
BKO
DISK-LOADED WAVEGUIDE
ZnS
ZnS
IP
OPTICS CHAMBER
ELEVATION

Fig. 9

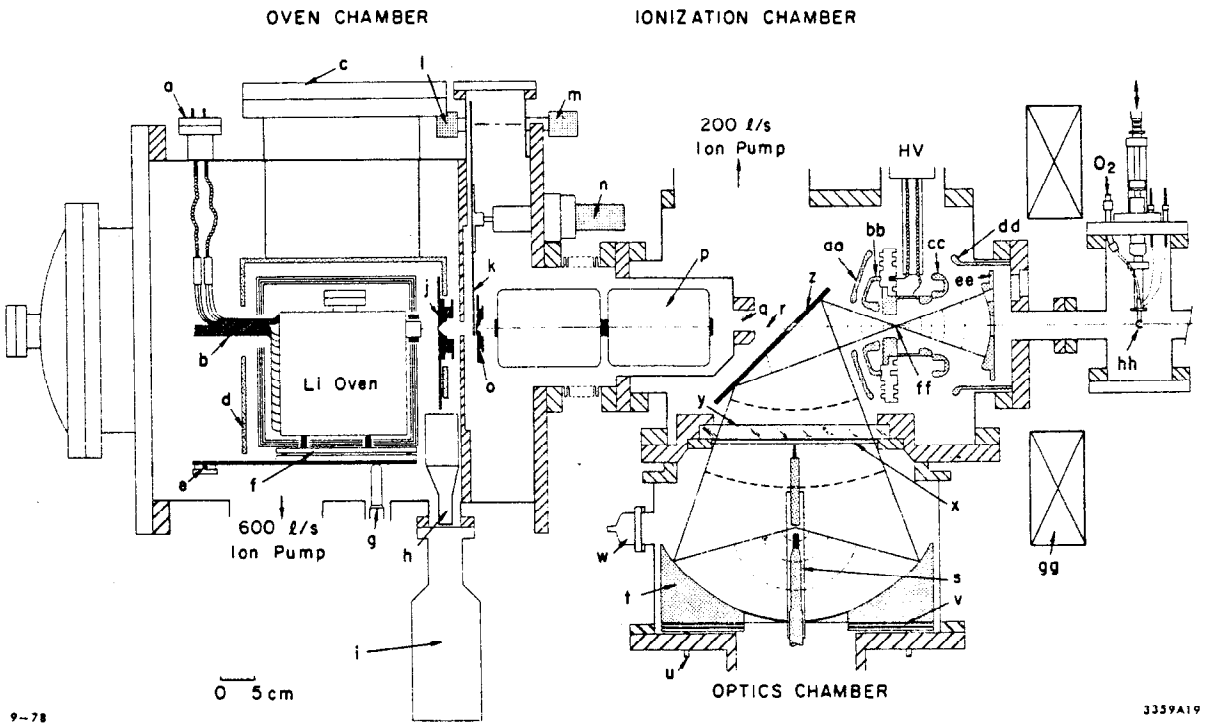
OVEN CHAMBER
IONIZATION CHAMBER
200 ℓ/s
Ion Pump
HV
O2
Li Oven
600 ℓ/s
Ion Pump
0 5 cm
OPTICS CHAMBER
9-78
3359A19

Fig. 10

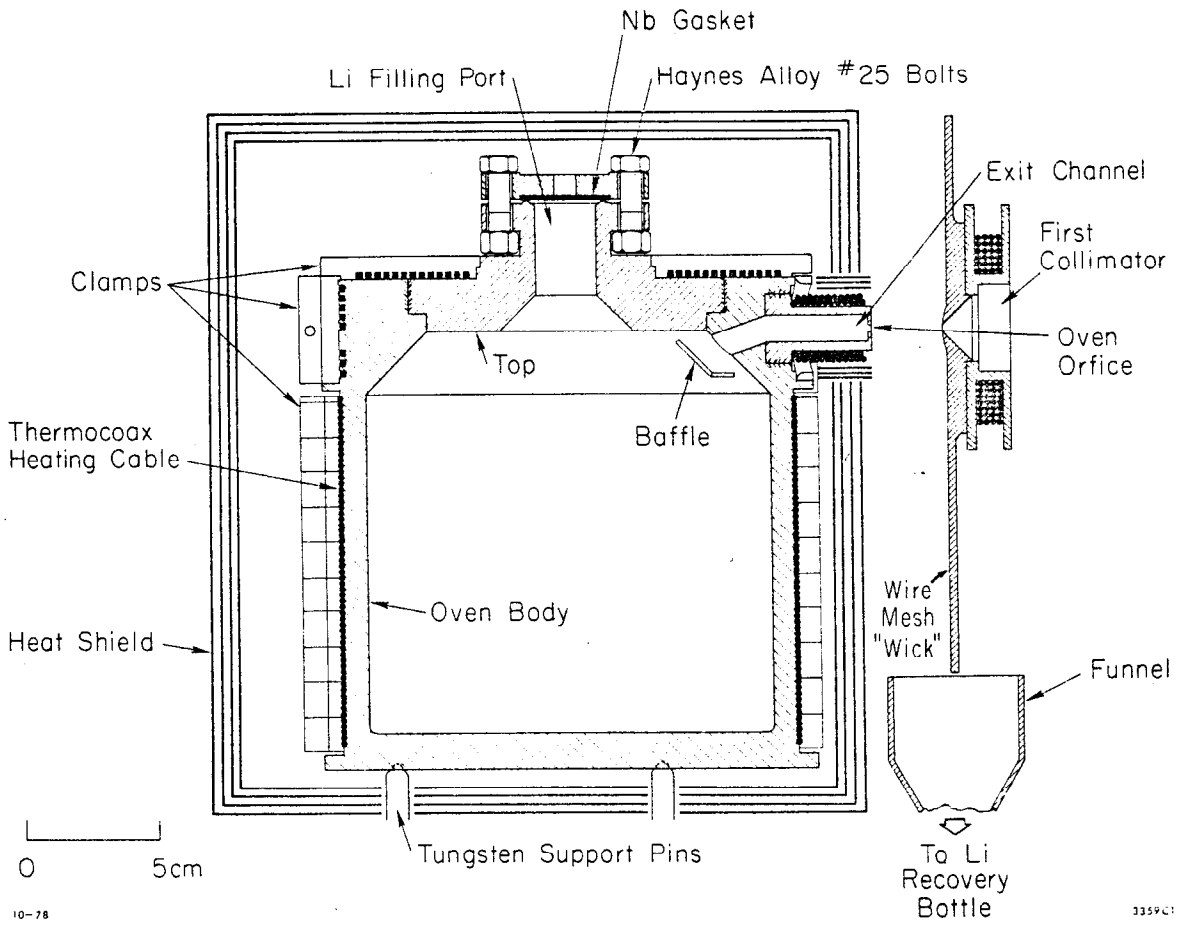
Nb Gasket
Li Filling Port
Haynes Alloy #25 Bolts
Exit Channel
First Collimator
Clamps
Oven Orfice
Top
Baffle
Thermocoax Heating Cable
Oven Body
Heat Shield
Wire Mesh "Wick"
Funnel
0
5cm
Tungsten Support Pins
To Li Recovery Bottle
10-78
3359C1

Fig. 11

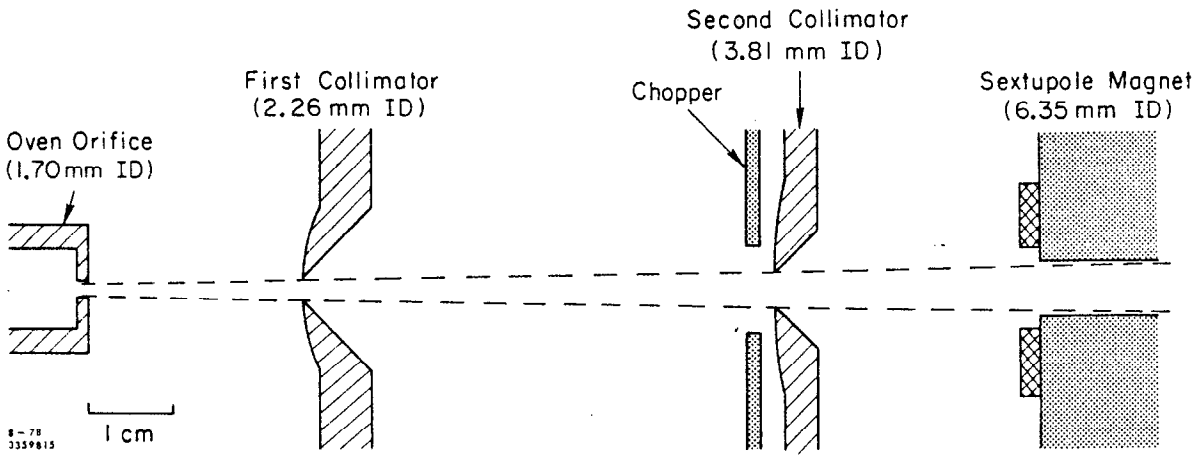
Second Collimator
(3.81 mm ID)
First Collimator
(2.26 mm ID)
Chopper
Sextupole Magnet
(6.35 mm ID)
Oven Orifice
(1.70mm ID)
1 cm
8-78
3339815

Fig. 12

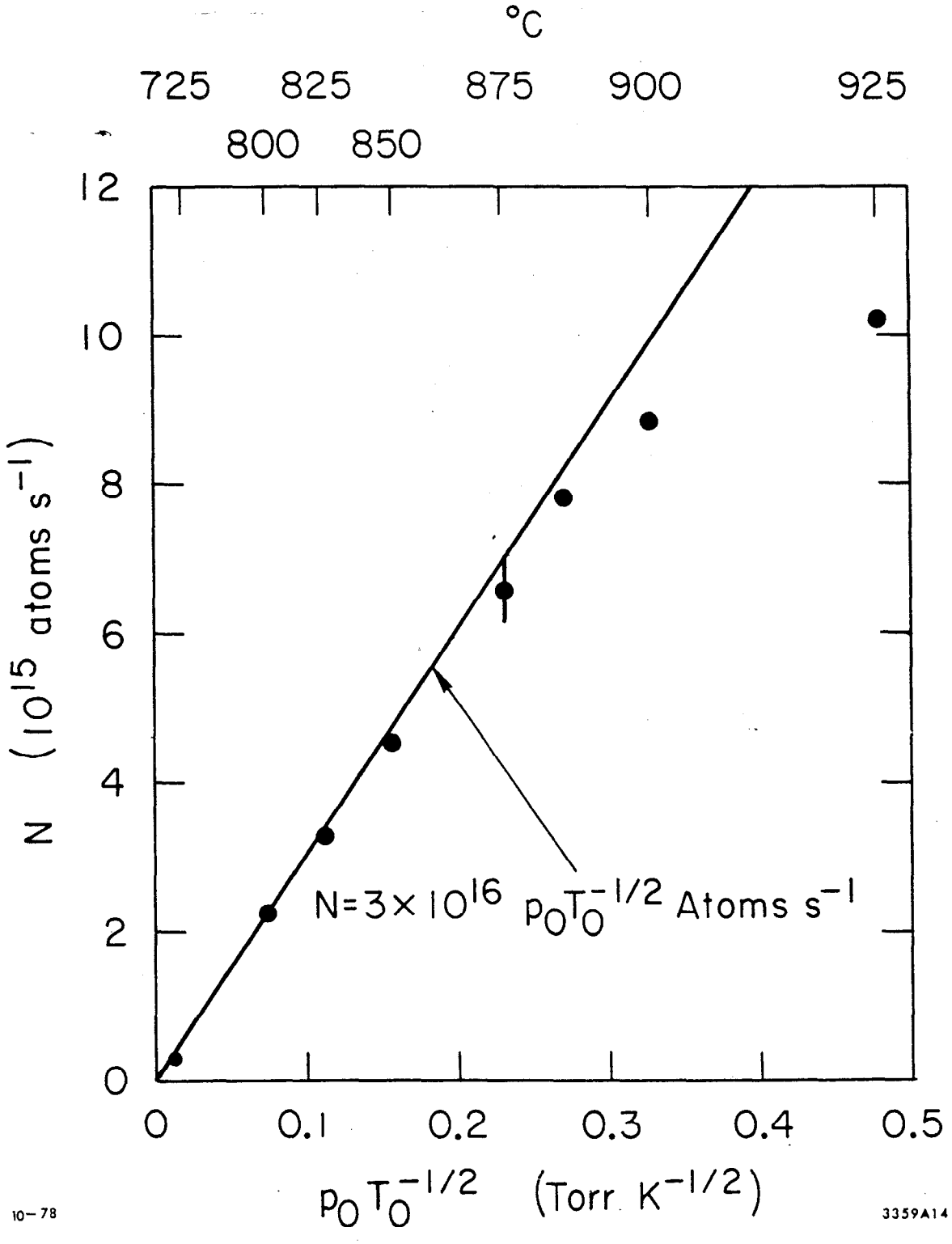
°C
725
825
875
900
925
800
850
12
10
8
6
4
2
0
N (10^15 atoms s^-1)
N=3×10^16 p0T0^-1/2 Atoms s^-1
0
0.1
0.2
0.3
0.4
0.5
p0 T0^-1/2 (Torr K^-1/2)
10-78
3359A14

Fig. 13

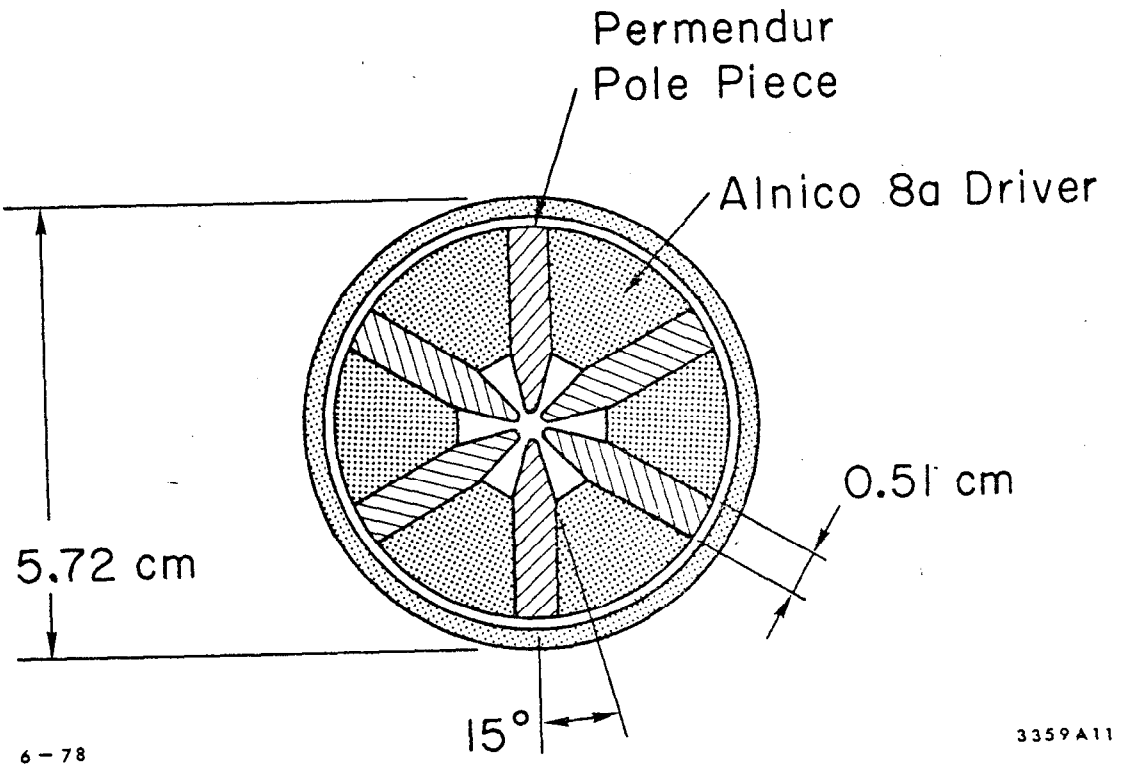
Permendur
Pole Piece
Alnico 8a Driver
0.51 cm
5.72 cm
15°
6-78
3359A11

Fig. 14

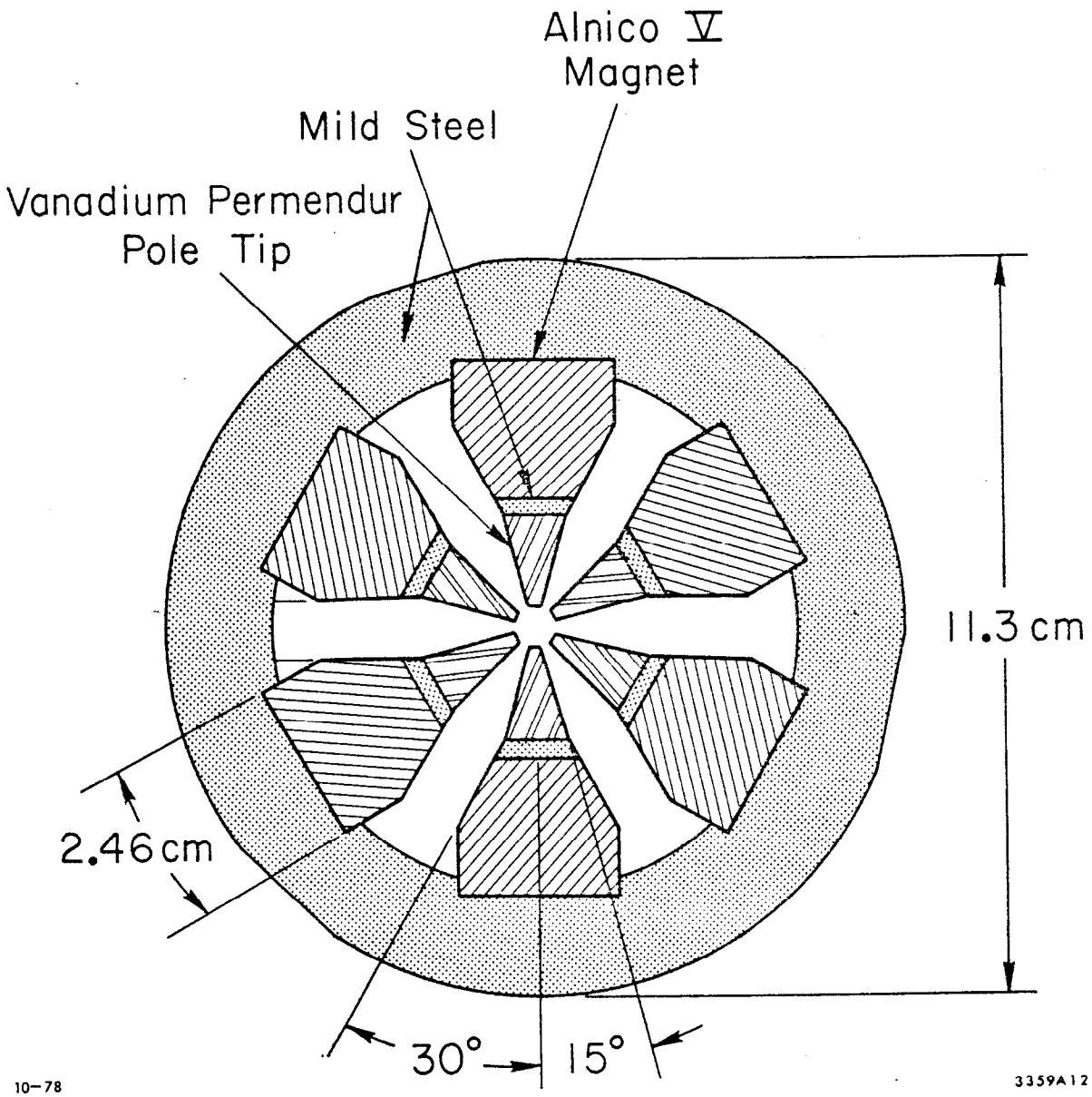
Alnico V
Magnet
Mild Steel
Vanadium Permendur
Pole Tip
11.3 cm
2.46 cm
30°
15°
10-78
3359A12

Fig. 15

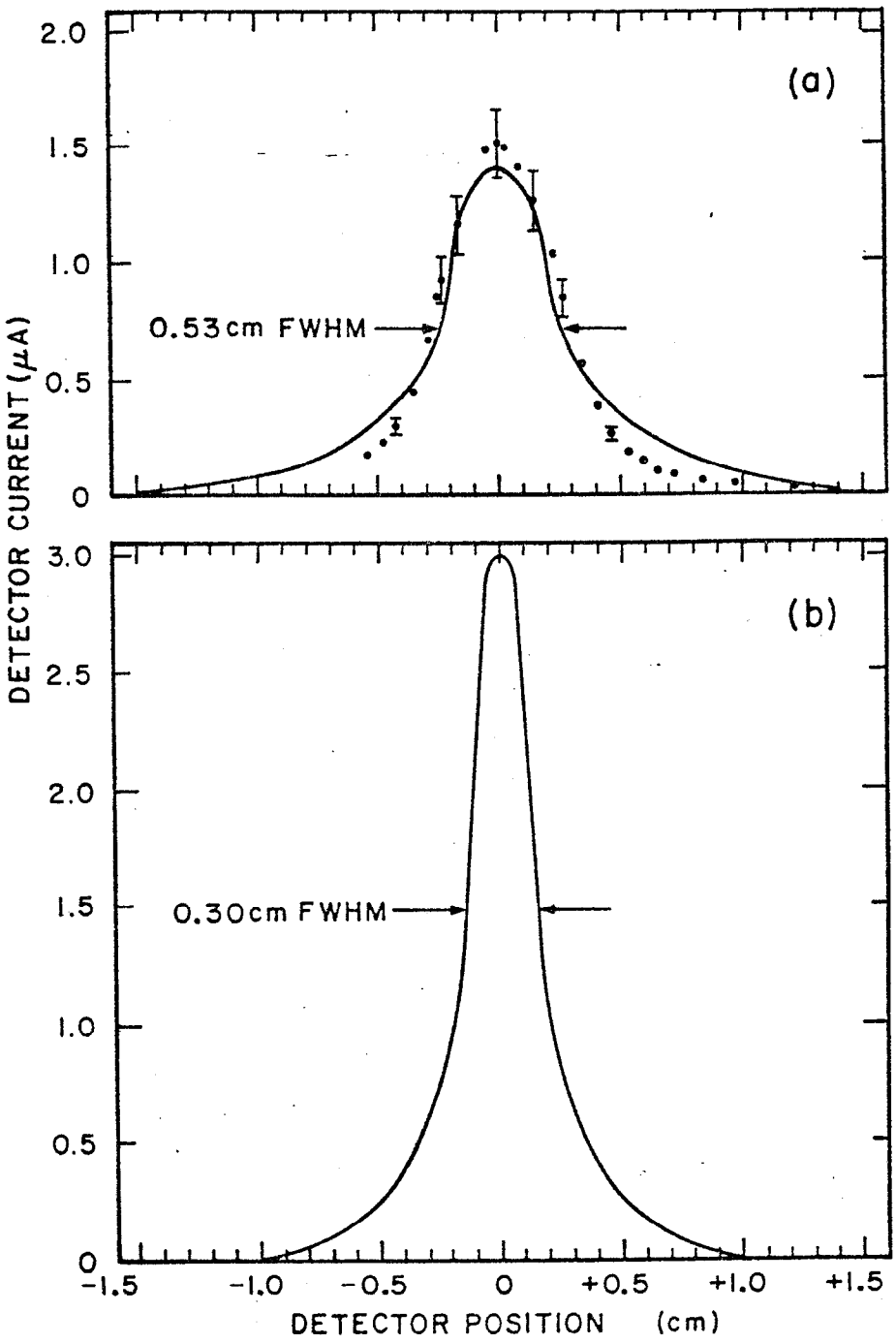
(a)
0.53cm FWHM
(b)
0.30cm FWHM
DETECTOR CURRENT (μA)
DETECTOR POSITION (cm)
2.0
1.5
1.0
0.5
0
3.0
2.5
2.0
1.5
1.0
0.5
0
-1.5
-1.0
-0.5
0
+0.5
+1.0
+1.5

Fig. 16

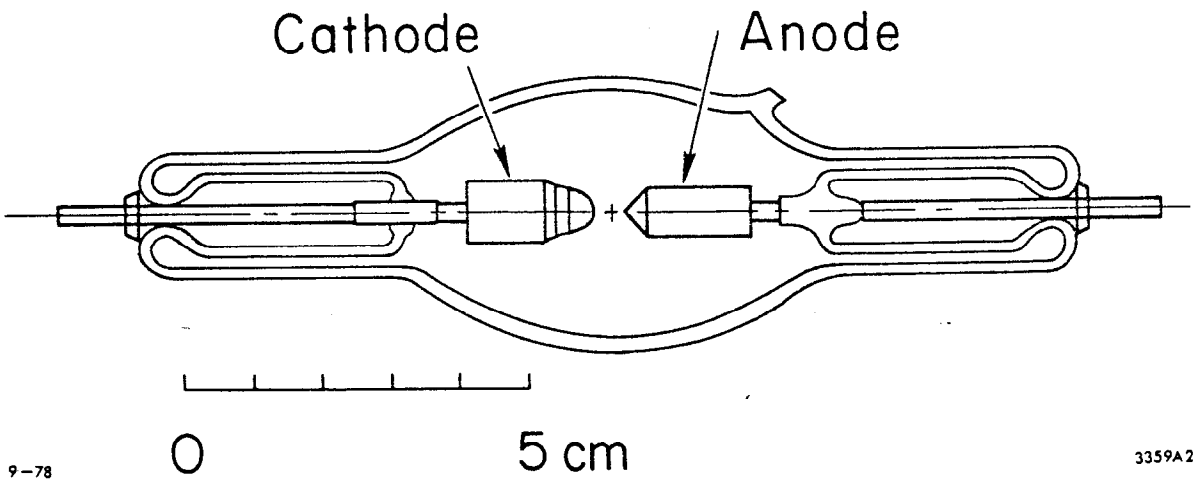

Fig. 17

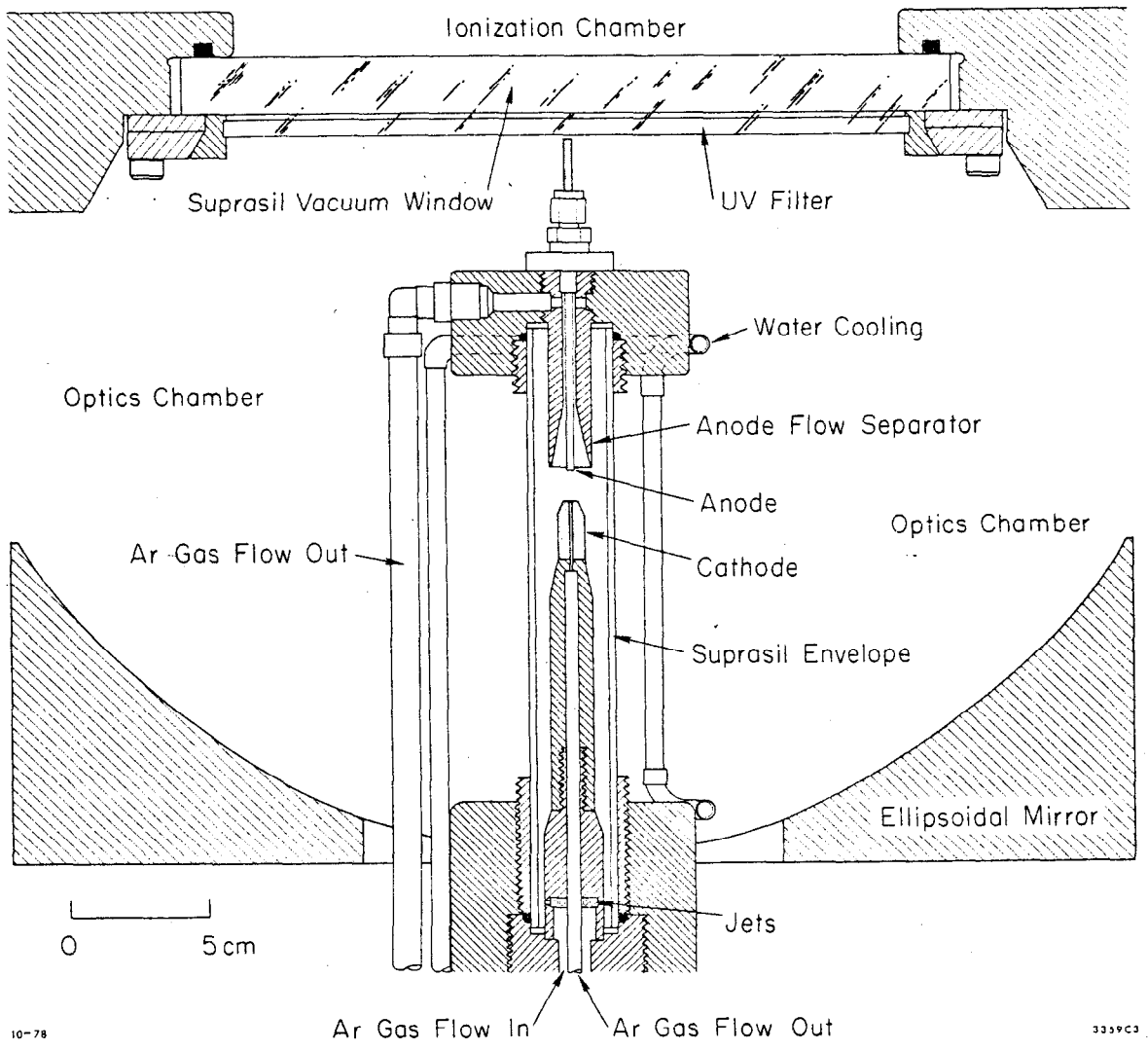
Ionization Chamber
Suprasil Vacuum Window
UV Filter
Water Cooling
Optics Chamber
Anode Flow Separator
Anode
Optics Chamber
Ar Gas Flow Out
Cathode
Suprasil Envelope
Ellipsoidal Mirror
0
5 cm
Jets
Ar Gas Flow In
Ar Gas Flow Out
10-78
3339C3

Fig. 18

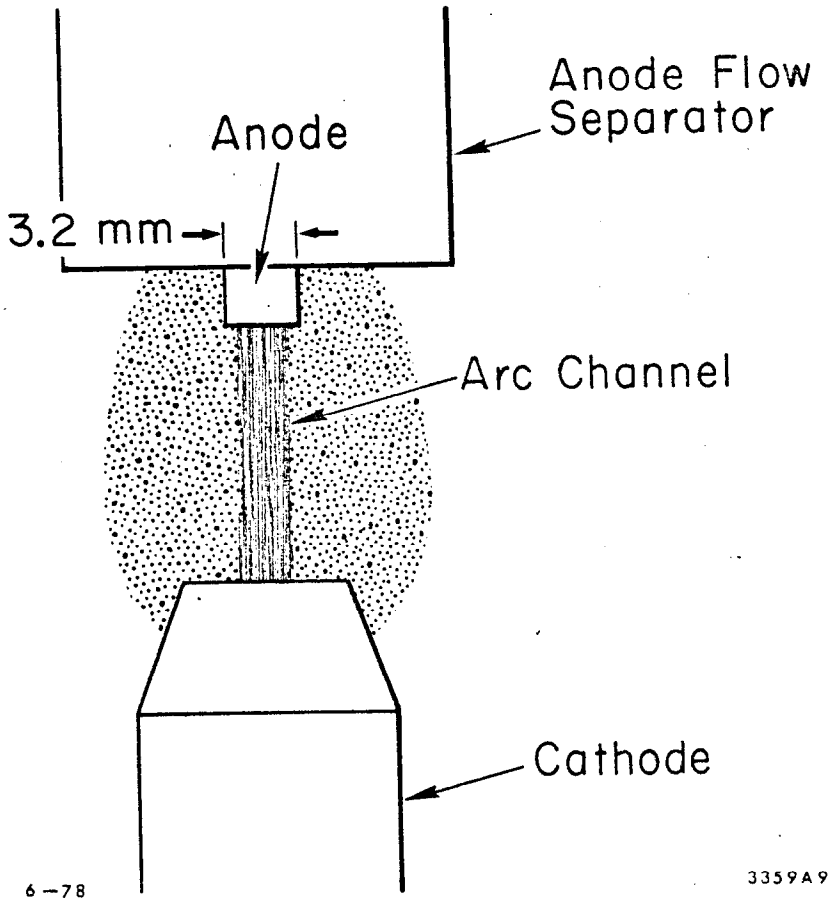
Anode Flow
Separator
Anode
3.2 mm
Arc Channel
Cathode
6-78
3359A9

Fig. 19

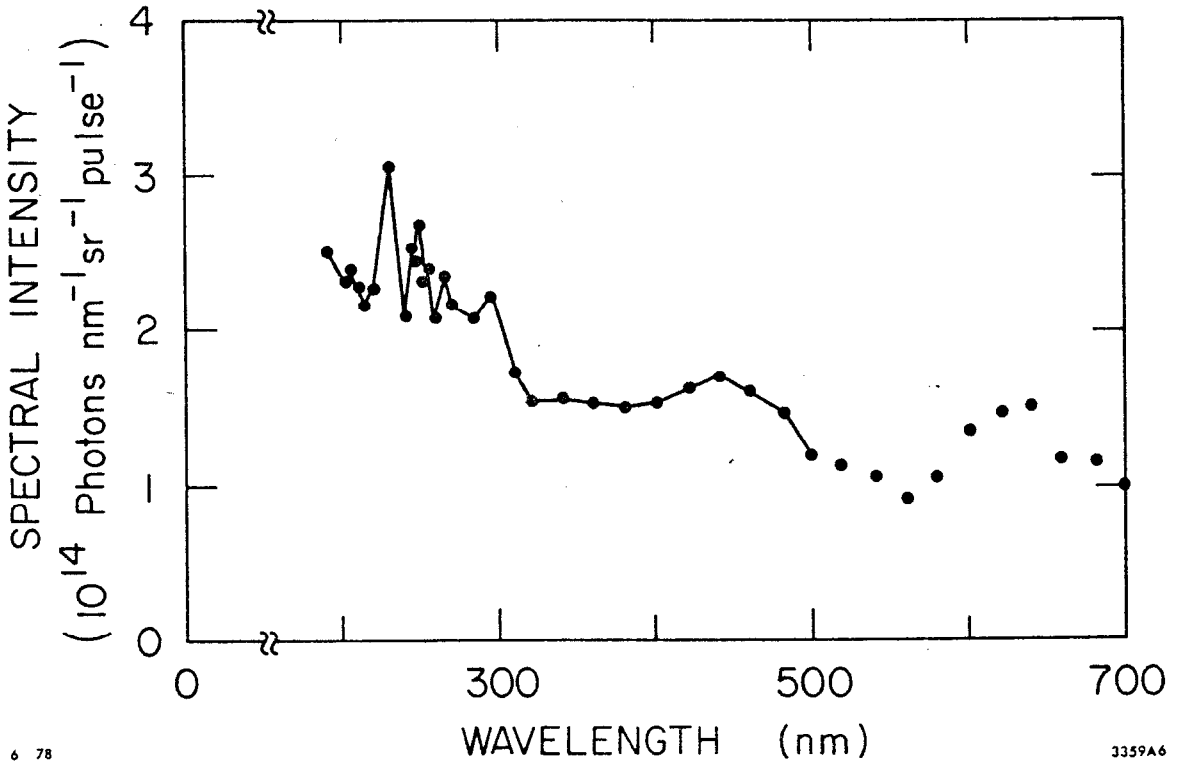
SPECTRAL INTENSITY
(10^{14} Photons $nm^{-1} sr^{-1} pulse^{-1}$)
4
3
2
1
0
0
300
500
700
WAVELENGTH (nm)
6 78
3359A6

Fig. 20

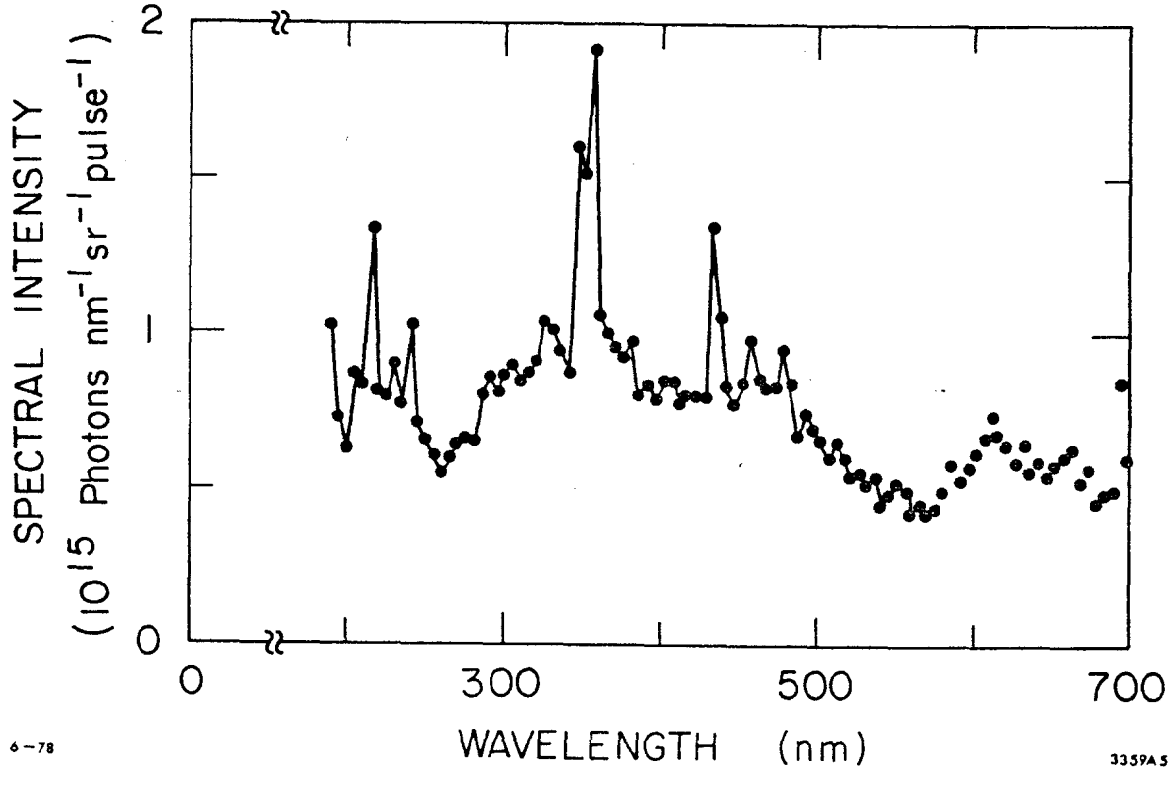
SPECTRAL INTENSITY
(10^{15} Photons $nm^{-1}sr^{-1}pulse^{-1}$)
2
1
0
0
300
500
700
WAVELENGTH (nm)
6-78
3359A5

Fig. 21

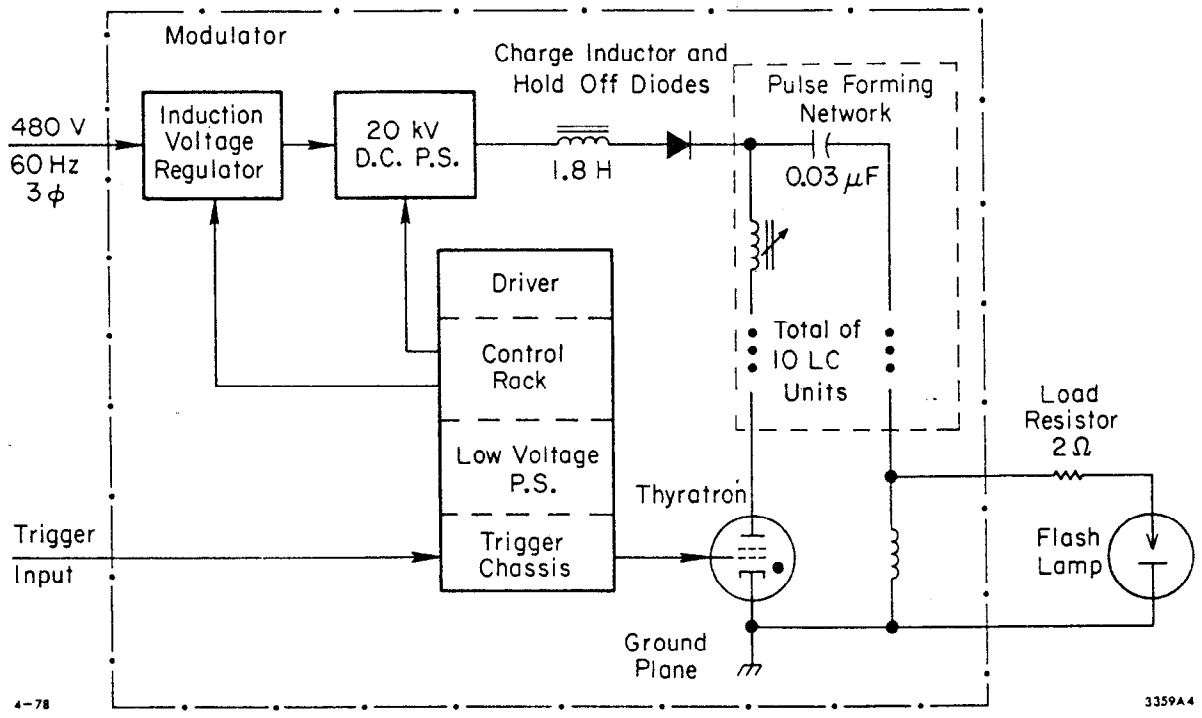
Modulator
480 V
60 Hz
3 ϕ
Induction Voltage Regulator
20 kV D.C. P.S.
Charge Inductor and Hold Off Diodes
1.8 H
Pulse Forming Network
0.03 μF
Total of 10 LC Units
Driver
Control Rack
Low Voltage P.S.
Trigger Chassis
Trigger Input
Thyratron
Load Resistor 2 Ω
Flash Lamp
Ground Plane
4-78
3359A4

Fig. 22

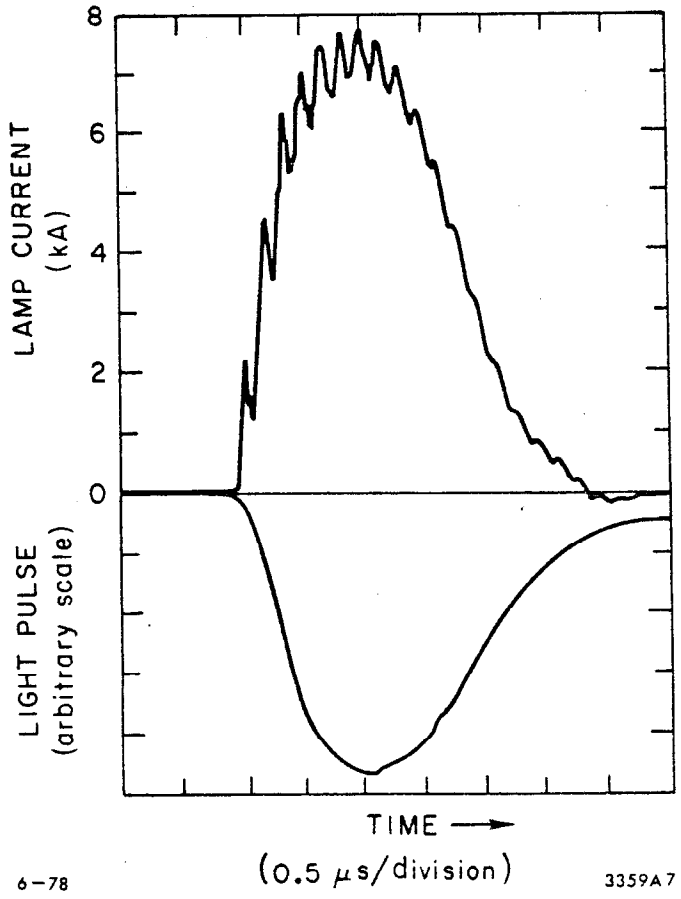
8
6
4
2
0
LAMP CURRENT
(kA)
LIGHT PULSE
(arbitrary scale)
TIME →
(0.5 μs/division)
6-78
3359A7

Fig. 23

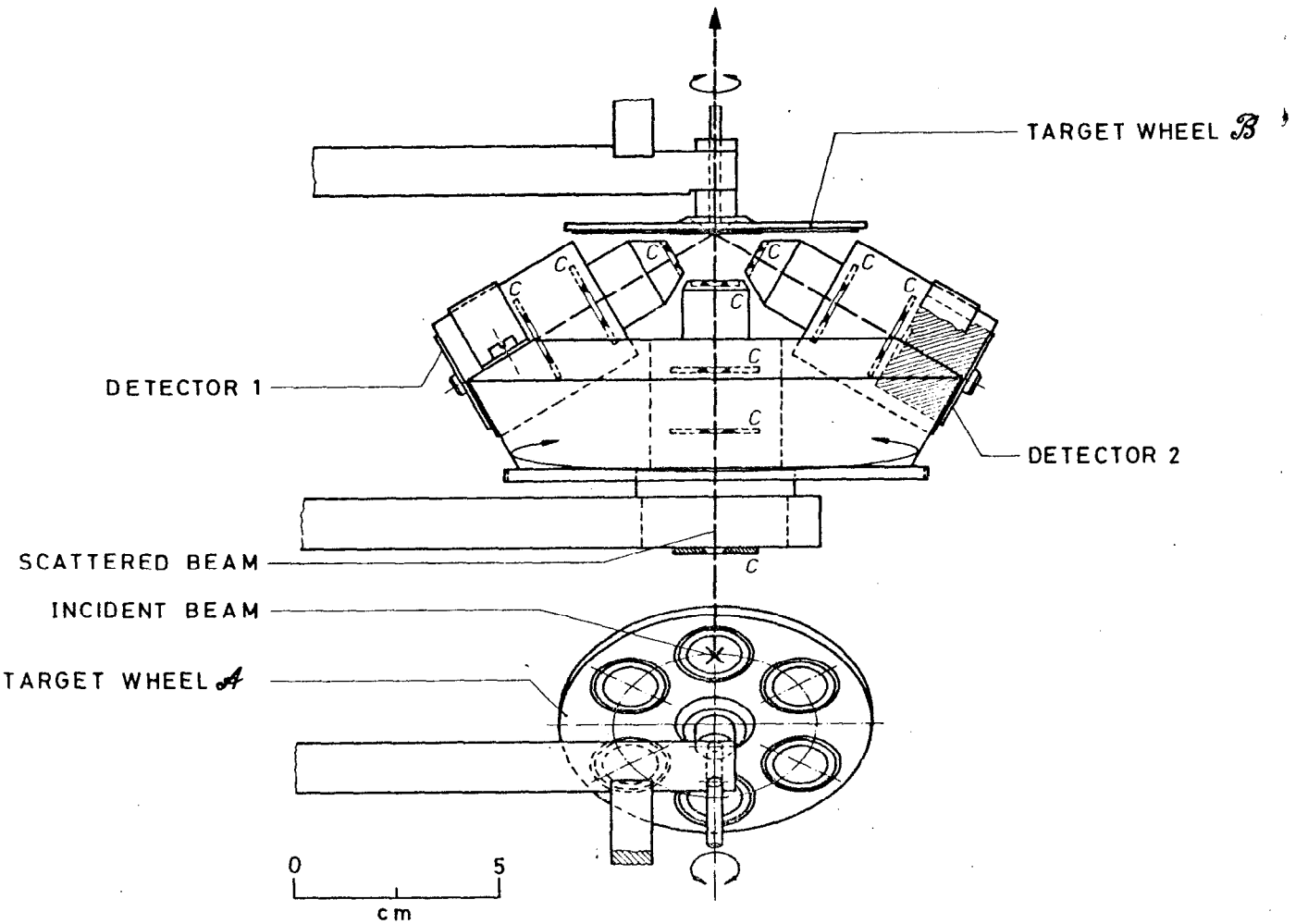
TARGET WHEEL B
DETECTOR 1
DETECTOR 2
SCATTERED BEAM
INCIDENT BEAM
TARGET WHEEL A
C
0
5
cm

Fig. 24

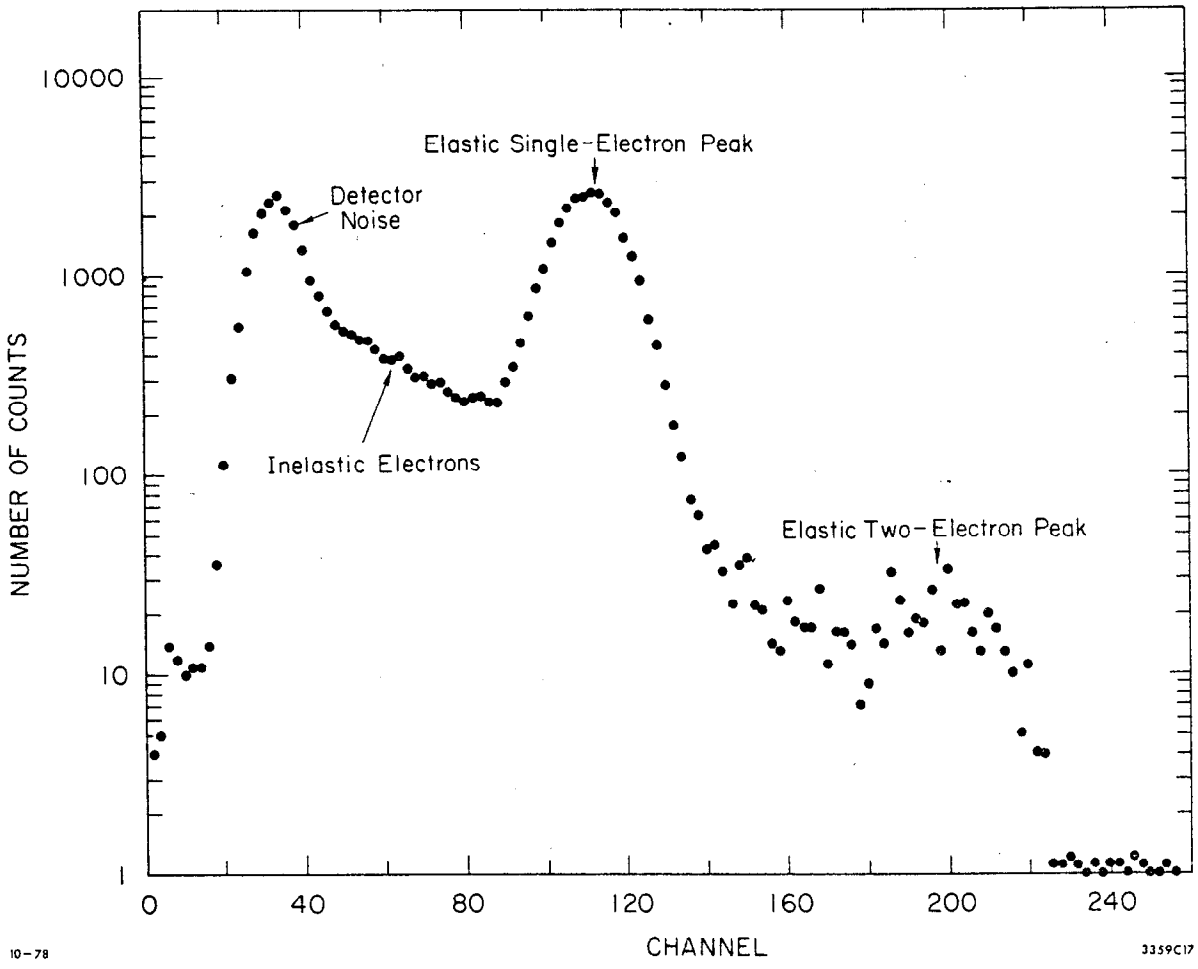
10000
1000
100
10
1
NUMBER OF COUNTS
Elastic Single-Electron Peak
Detector
Noise
Inelastic Electrons
Elastic Two-Electron Peak
0
40
80
120
160
200
240
CHANNEL
10-78
3359C17

Fig. 25

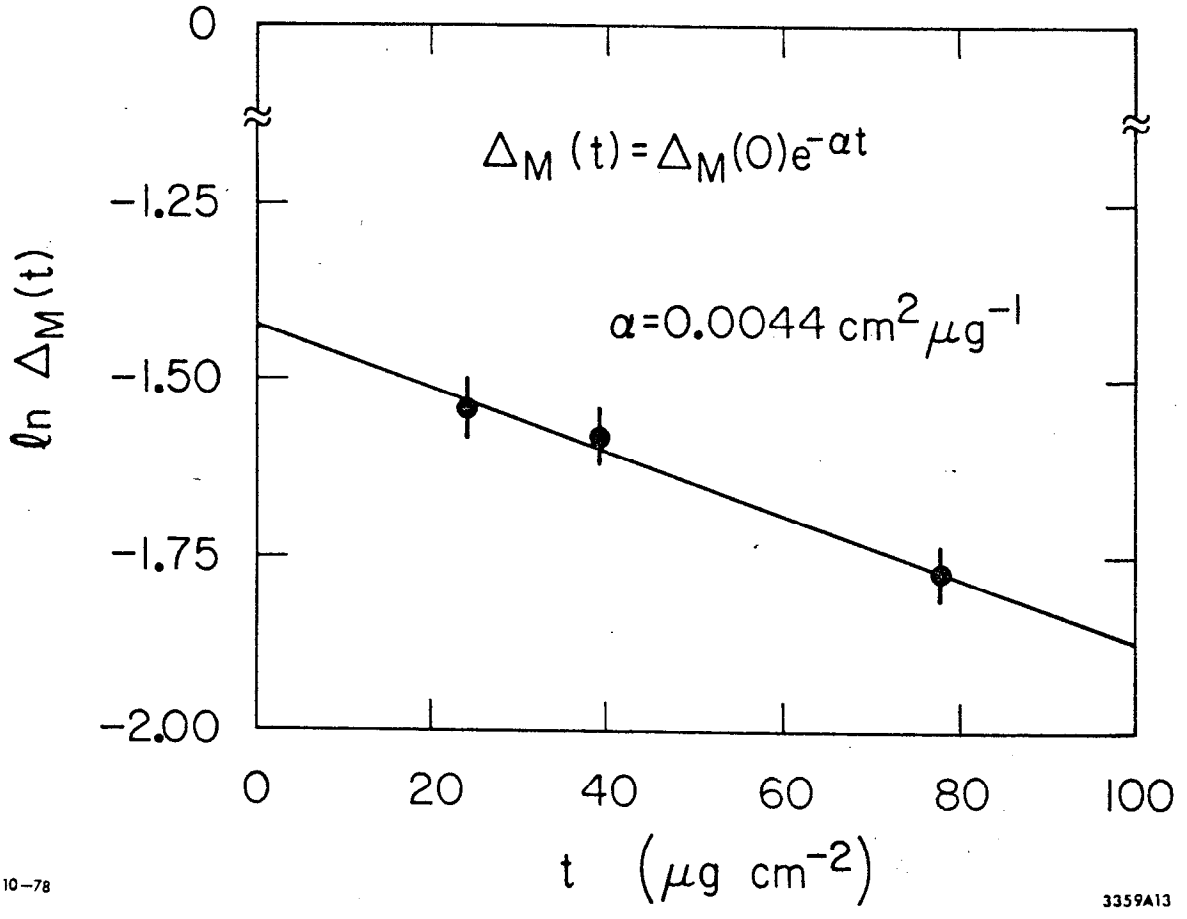
0
-1.25
-1.50
-1.75
-2.00
ln $\Delta_M(t)$
$\Delta_M(t) = \Delta_M(0)e^{-\alpha t}$
$\alpha = 0.0044\ cm^2 \mu g^{-1}$
0
20
40
60
80
100
t $(\mu g\ cm^{-2})$
10-78
3359A13

Fig. 26